

Review

# Large-Power Transformers: Time Now for Addressing Their Monitoring and Failure Investigation Techniques

Jonathan Velasco Costa <sup>†</sup>, Diogo F. F. da Silva <sup>†</sup> and Paulo J. Costa Branco <sup>\*†</sup> 

IDMEC, Instituto Superior Técnico, Universidade de Lisboa, 1049 Lisbon, Portugal; jonathanvelasco@tecnico.ulisboa.pt (J.V.C.); diogo.d.silva@tecnico.ulisboa.pt (D.F.F.d.S.)

\* Correspondence: author: pbranco@tecnico.ulisboa.pt

<sup>†</sup> These authors contributed equally to this work.

**Abstract:** Several review studies exist in the literature about monitoring, fault detection, and diagnosis of power transformers. However, they are general approaches in terms of power transformers. Some only focus on applying a specific class of techniques, but again, for general power transformers. Other reviews focus on applying different technologies such as fiber optics, thermal cameras, and vibration sensors, but all within the perspective of general power transformers. A significant question remains: among all types of power transformers, which specific techniques should be used, and why are they more adequate? What are the uncertainties that can decrease their precision? What about the balance, in terms of costs, associated with applying a certain technique and the return needed for a particular type of transformer? In this context, this paper is not only a literature review of well-known problems related to power transformers. Here, we do not just center on large power transformers (100 MVA or higher). Still, we describe a case study of a phase-shifting 1400 MVA-400 kV three-phase transformer that currently connects two European countries that began to show signs of abnormal operating conditions in 2012. In this way, the need to detect and identify anomalies in their initial stage of development for a possible preventive maintenance action is more than justified, which is essentially achieved with continuous monitoring models of the transformer, as concluded in this paper.

**Keywords:** large power transformer; condition monitoring; transformer fault diagnosis; diagnostic techniques; mechanical or electrical integrity of the core and windings



**Citation:** Costa, J.V.; Silva, D.F.F.d.; Branco, P.J.C. Large-Power Transformers: Time Now for Addressing Their Monitoring and Failure Investigation Techniques. *Energies* **2022**, *15*, 4697. <https://doi.org/10.3390/en15134697>

Academic Editors: Philip Pong, Weiqiang Dong, Moshe Kam and Federico Barrero

Received: 11 March 2022

Accepted: 6 May 2022

Published: 27 June 2022

**Publisher's Note:** MDPI stays neutral with regard to jurisdictional claims in published maps and institutional affiliations.



**Copyright:** © 2022 by the authors. Licensee MDPI, Basel, Switzerland. This article is an open access article distributed under the terms and conditions of the Creative Commons Attribution (CC BY) license (<https://creativecommons.org/licenses/by/4.0/>).

## 1. Introduction

Large power transformers (LPT) are custom-built pieces of equipment that are crucial links to the bulk transmission grid. Usually, they link a generator-transmission line and/or linking lines of different voltages. LPTs are characterized by technical and logistic features, making them a special case for condition monitoring of power transformers. These features are:

1. LPTs are usually neither interchangeable nor produced for extensive spare inventories since they are very expensive and tailored to customers' specifications. LPTs can cost millions of euros, and each device weights between approximately 100 and 400 tons [1];
2. Replacing an LPT after a failure can be difficult because of the limited availability of spare devices. This is a potential issue regarding the required resilience of the power grid [2,3];
3. Unfortunately, being a piece of custom-built equipment, the production process of LPTs can extend beyond 20 months if, for example, the manufacturer has difficulty obtaining certain key parts or materials for LPT's production (ex: acquisition of special grade electrical steel);
4. The average age of installed LPTs in the United States and Europe is over 20 years [4]. While the life expectancy of a power transformer varies depending on how and where

it is used, aging power transformers are potentially subject to an increased risk of failure. Figure 1 shows how age increases the transformer failures rate when installed in industrial plants, generation plants, and transmission networks. The failure rate curves are sharper for industrial and generator transformers because the transformers in these installations tend to be exploited more intensively.

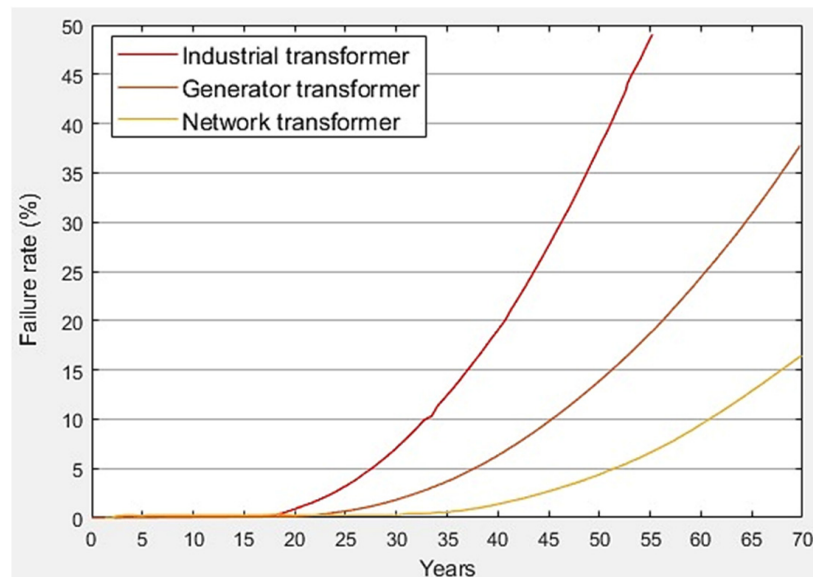


**Figure 1.** Aging increases the LPTs failure rate when installed in industrial plants, generation plants, and transmission networks (adapted from [5]).

According to [6], LPTs are in general divided into transmission transformers, with the low voltage side rated 100 kV or higher and the maximum nameplate rating 100 MVA or higher; and generation set-up transformers, with high voltage side, rated 100 kV or higher and the maximum nameplate rating 75 MVA or higher. Figure 2 illustrates a standard core-type LPT and its major internal components.

1. Three-limb core
2. LV Winding
3. HV Winding
4. Tapped Winding
5. Tap Leads
6. LV Bushings
7. HV Bushings
8. Clamping Frame
9. On-Load Tap Changer
10. Motor Drive
11. Tank
12. Conservator
13. Radiators

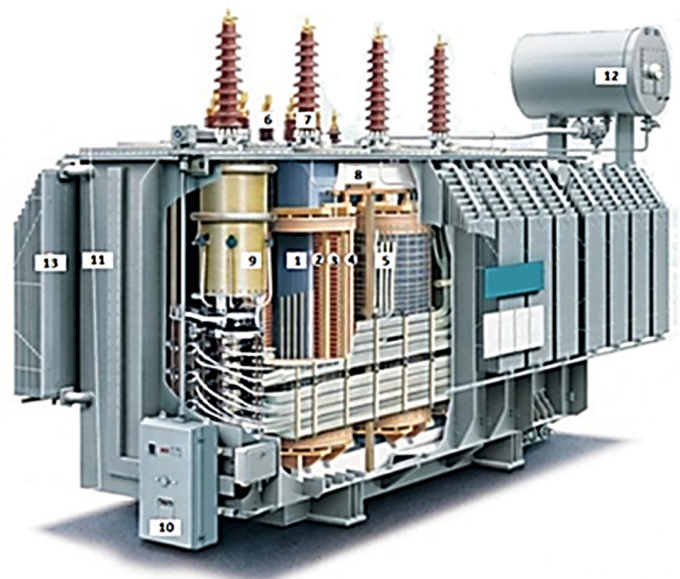


**Figure 2.** Standard core-type large power transformer and its major internal components.

The LPT key characteristics are large, tailored to certain customer specifications, expensive, rarely interchangeable, or produced for extensive spare inventories. To understand

how LPTs can differ in some aspects, a localized power outage at the distribution level (distribution transformers) will not present significant reliability threats. Utilities often maintain spare transformer equipment of their size range. An outage of an LPT is completely out of this reality. Figure 2 illustrates a standard core-type LPT and its major internal parts and components: the core, which is made of high-permeability, grain-oriented, silicon electrical steel laminations; the electrical input-output windings, which are made of copper conductors wound around the core; the tank where core and windings are contained; the bushings connecting the LPT to transmission line; the tap-changer, power cable connectors, gas-operated relays, thermometers, relief devices, dehydrating breathers, oil level indicators, and other controls.

One must recognize several review studies in the literature on monitoring, fault detection, and diagnosis of power transformers. However, those reviews are general approaches in terms of power transformers as recent examples of reviews published in [7–11], reviews focusing on the application of a specific class of techniques again for general power transformers as in [12–14], and reviews centered in applying different technologies like fiber optics in [15], thermal cameras in [16], vibration sensors in [16,17], but all within general power transformers' perspective.

The question that one has to put today is: among all types of power transformers, which specific techniques to use, and why are they more adequate? What are the uncertainties that can decrease their precision? What about the balance of costs associated with applying a certain technique and the return needed for a particular type of transformer?

In this context, this review is not only a literature review of well-known problems related to power transformers. We not only center on large power transformers (100 MVA or higher), but we use a case study of a phase-shifting 1400 MVA-400 kV three-phase transformer connecting two European countries that began to show signs of abnormal operating conditions in 2012. From this perspective, it is more than justified for LPTs to detect and identify failures at their early stage to implement preventive actions, which is achieved mainly through continuous monitoring of the transformer. In addition, if the LPT condition of this equipment is continuously monitored in time, it is possible to manage its life cycle. In other words, it will be possible to define maintenance actions based on the condition of this critical asset rather than providing preventive maintenance, which is nowadays the common practice and is carried out at specific time intervals.

The present paper summarizes large power transformers' particularities of monitoring and diagnosis for these assets. Unlike other similar reviews, this will mirror the authors' experience with a 1400 MVA phase-shift LPT in service since 2007 manufactured by ABB with a nominal voltage on the primary and secondary side of 400 kV phase-shifting within  $\pm 25^\circ$ .

## 2. Oil-Immersed Large Power Transformers: Abnormal Operating Conditions

In the current context of deregulation of electricity systems and mainly under the conditions mentioned in the introduction, each electricity company seeks to manage its assets more efficiently, basing itself on conditional and proactive maintenance methodologies. This pursues to limit the number of interruptions in the grid and thus avoid economic penalties that can be severe. More specifically, only one large power transformer's shutdown can lead to direct and indirect losses that would far exceed its price [7].

It is even more essential for large power transformers to understand which condition of their components indicates an *abnormal operation*. To systematize this point, it is shown in Figure 3 a drawing cut of a typical large power transformer and its main components. The potential and associated abnormal conditions are presented based on those identified.

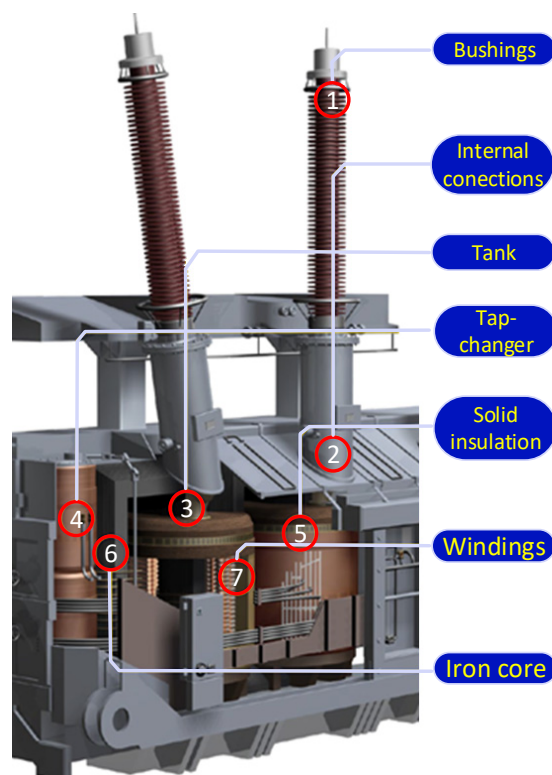


**Figure 3.** A large power transformer and its main components.

## 2.1. Active Part

### 2.1.1. Windings

The windings' abnormal operating conditions are one of the most frequent causes of failures, for they can experience wear at the mechanical, thermal, and dielectric levels [18]. These three always appear in a coupled way, and, most often, one of the phenomena proves to be more significant for the appearance of failure.

Mechanical anomalies are the windings' loosening, displacement, or deformation [19,20], as shown in Figure 4a. These anomalies originate from improper repair, poor maintenance, corrosion, manufacturing defects, vibrations, and mechanical displacements within the transformer. On the other side, windings can present high thermal losses in events such as a short circuit in the outer terminals. These losses usually give rise to "hot spots" that can lead to small ruptures or even the total copper breaking in the windings.

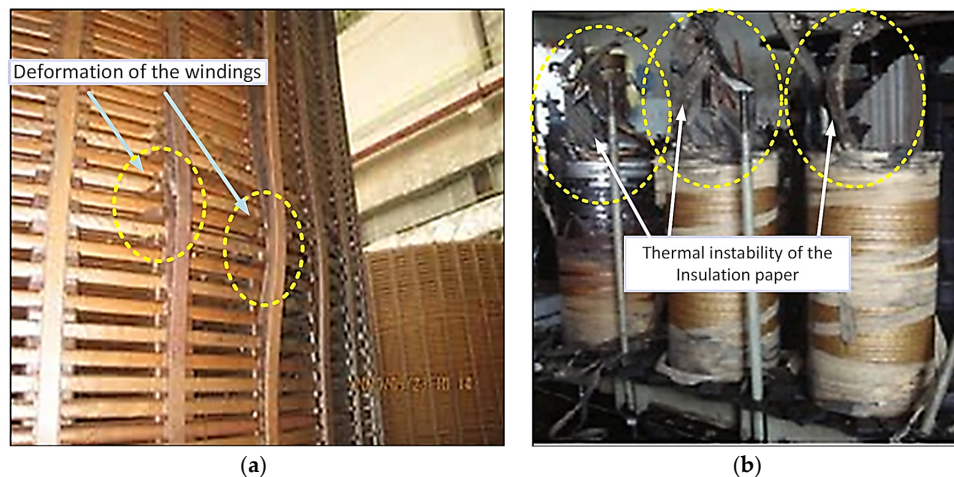


**Figure 4.** Examples of abnormal conditions in the windings, in (a) [18], there is a deformation of the windings. In (b) [19], there is a dielectric failure (poor condition of the insulation paper).

Dielectric anomalies come from disruptions of the insulating material between phases. Disruption occurs due to high potential differences such that the resulting electric field causes ruptures within the dielectric material. These can occur between turns of the same phase or between phases. Often, disruption will result in the appearance of small, short circuits that will lead to local burning of the windings [21], as shown in Figure 4b.

### 2.1.2. Transformer Core

One of the most frequent defects in the core [22] is shown in Figure 5. The displacement of the core blades due to electromagnetic forces is verified due to high eddy currents that circulated in them. In this situation, each conductor (blade) with an induced current produces a magnetic field that, when interacting with the currents circulating in the opposite blade, provokes electromagnetic forces in it, which causes a deformation in the plates [19]. Figure 6 shows an illustration of this phenomenon. If the laminations presented induced currents circulating in opposite directions, this would cause the appearance of repulsive electromagnetic forces, as in Figure 5, otherwise appear attractive forces between laminated sheets.

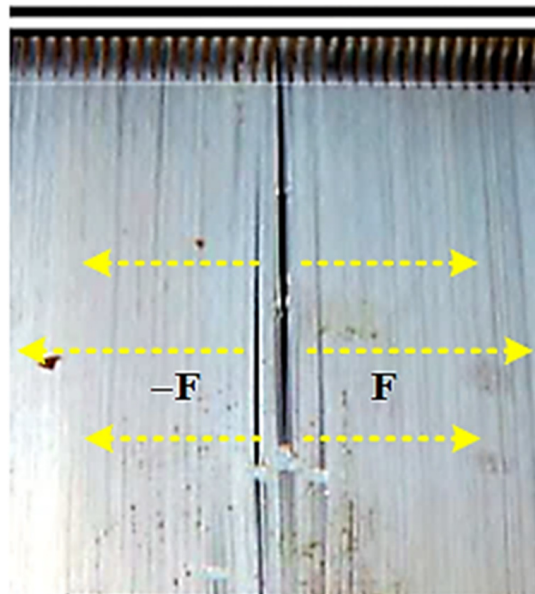


**Figure 5.** Illustration of a power transformer case presenting mechanical deformation of the core and laminated electrical sheets [21].

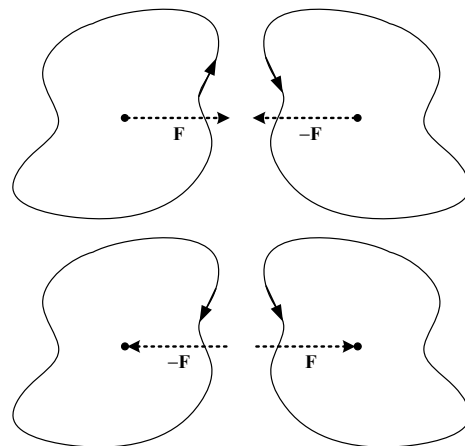


**Figure 6.** Illustration of forces according to the current direction.

## 2.2. Insulation System

### 2.2.1. Solid Insulation

Solid insulation is based on cellulose, namely paper and pressed wooden impregnated with oil forming a dielectric and mechanical insulation of the windings. The abnormal operating conditions that arise in these elements result mainly from the degradation of cellulose. The degradation has three mechanisms as its basis: hydrolysis (decomposition of the chemical compound by reaction with water), pyrolysis (decomposition or transformation of the compound by the action of heat), and oxygenation (combination of a substance with oxygen) [23]. The hydrolysis phenomenon is the mechanism that contributes most to the breakdown of the long chains of glucose rings that make up cellulose. This degradation and aging of cellulose significantly contribute to the loss of dielectric and mechanical properties that lead, for example, to short circuits between windings.

### 2.2.2. Liquid Insulation

The dielectric fluid has two objectives: insulating the transformer core and its tank and cooling the transformer by convection. The oil circulates through the main tank, absorbed by the paper (helps its cooling), giving it special dielectric characteristics. Oil circulation also allows the removal of heat from the core to the environment, as the oil, when heating, rises and enters the pipe that leads to the radiator.

The quality of the used oil greatly affects the properties of the insulation and cooling systems as particles (water, rust, and acids) appear in it due to its aging [24,25]. These make the oil more viscous, making its circulation difficult, thus risking the transformer's cooling capacity. If these particles are electrical conductors, such as water, they can facilitate short-circuits between elements, representing a failure of the insulation system.

## 2.3. Components and Accessories

### 2.3.1. Bushings

Another type of transformer anomaly occurs in their *bushings* (Figure 7), which serve as insulation between the passage of the outer conductors and the interior connection to the windings; they act as a path for each stage's current through the walls of the tank.

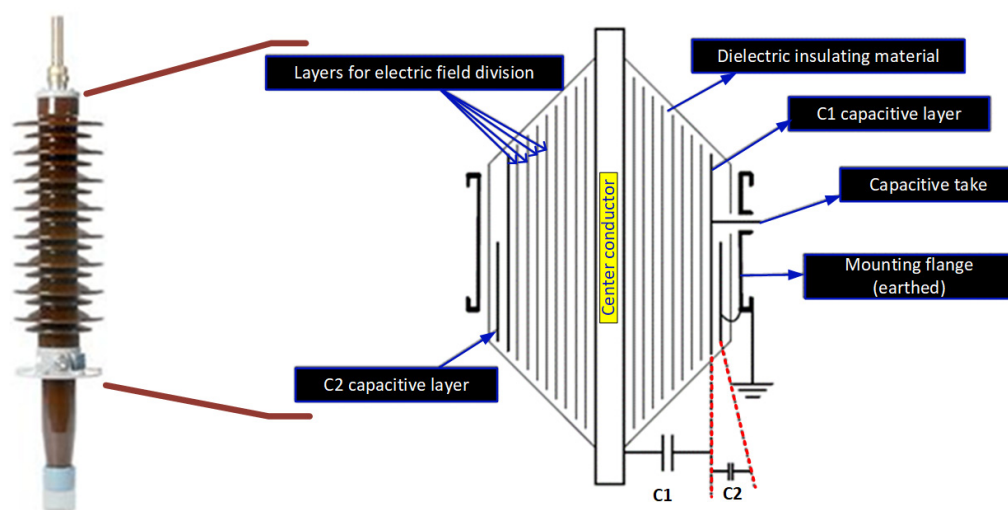


Figure 7. OIP bushing and capacitive bushings scheme.

The bushings can be of the capacitive or non-capacitive type, and for transformers, with higher operating voltages, it is usual to use the capacitive type bushings (Figure 7). Capacitive type *bushings* are classified as “OIP” (Oil Impregnated Paper—layers of oil-impregnated paper), “RIP” (Resin Impregnated Paper—paper impregnated with epoxy resins), and “RBP” (Resin Bonded Paper—layers of Bakelitized paper), the manufacture of the latter being practically abandoned due to problems related to partial discharges [26].

In Figure 7 left, it is possible to visualize an OIP bushing, and in Figure 7 right, it represents its scheme. The bushing is composed of a central conductor covered with paper impregnated in oil or resin (considering only the bushings of the OIP and RIP type) and the external insulator, usually in porcelain. The bushing is represented by a center conductor and several condensers between this and the mounting flange, as represented in its diagram in Figure 7, right side. Between the central conductor and the capacitive tap (where measurements are taken), there is the capacitor C1, which represents the value of the total capacitance in series resulting from the different layers of electric potential distribution. The capacitor C2 translates the capacitance value between the capacitive layer C2 and the capacitive tap; it corresponds to the insulation between C1 and the mounting flange [17].

Degradation of bushings, mainly those located at the high-voltage side, is reflected in the appearance of partial discharges and the loss of dielectric properties that will lead to overheating, as illustrated in Figure 8. This degradation may be due to the following set of factors:

1. Contamination of insulators, due to deposition of contaminants (water, dust) on the surface of bushings [27] and, for highly polluted places, they must be washed regularly;
2. Water ingress, which can enter, for example, through small cracks in the porcelain, which can be the result of mechanical damage to the bushing or else due to the bushing swelling and deflating with temperature [14,28];
3. Aging process of the bushing [29,30].

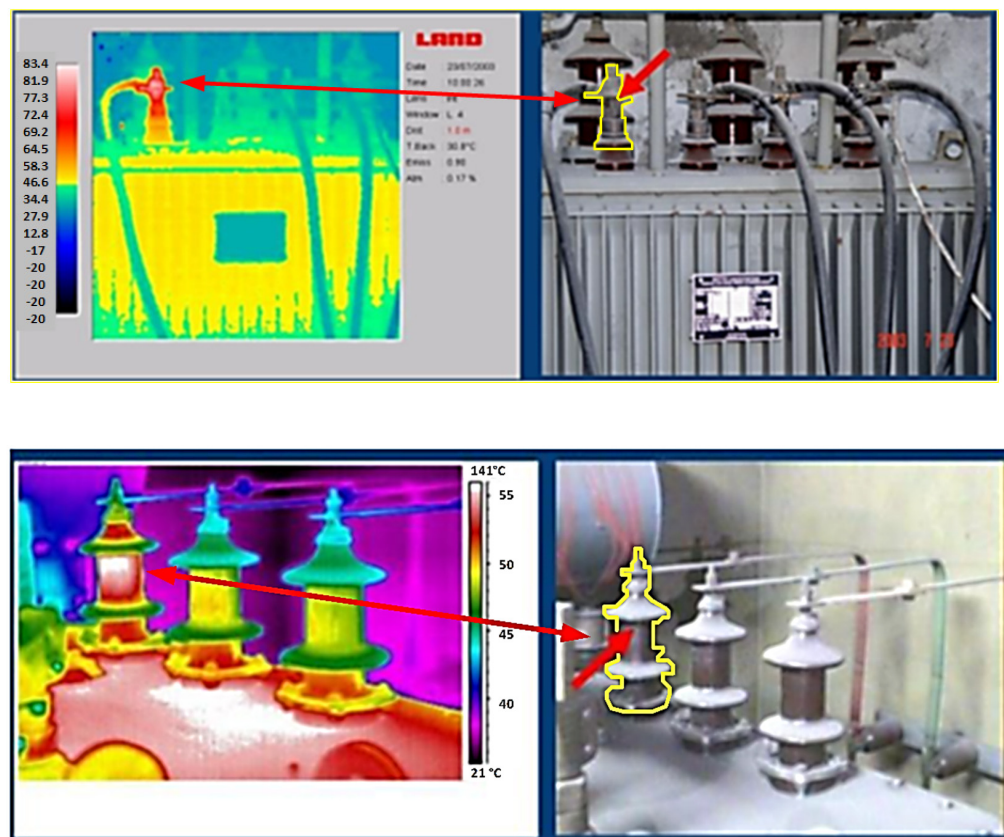
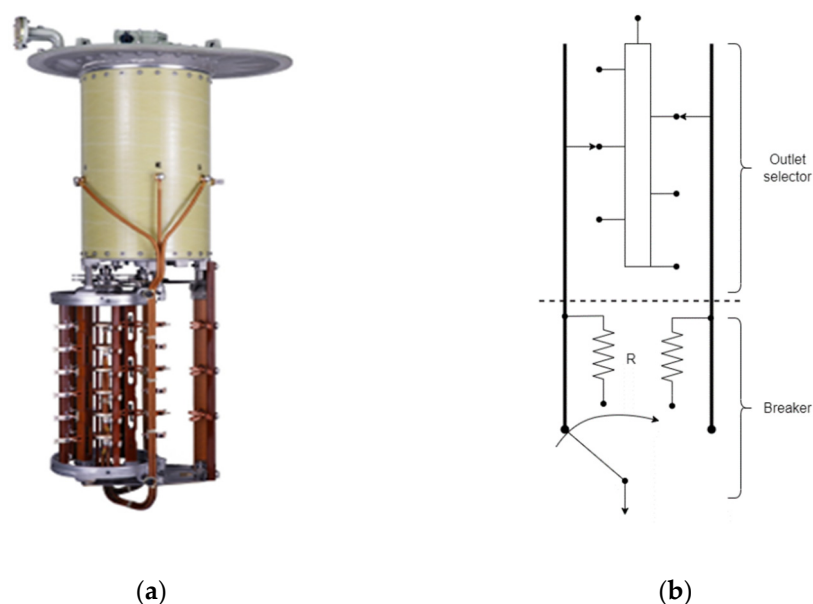


Figure 8. Thermographic photographs of overheating bushings [31].

### 2.3.2. Tap-Changer

Tap-changer is one of the most critical components of a large power transformer [32] as it is one of the only that exhibits a controlled displacement (Figure 9a). It can regulate the voltage and/or phase change by varying the ratio of the number of turns of the transformer without interrupting the load, thus compensating for constant load variations. There are

two types of tap-changers: those using resistors or reactances during the switching process. The first is installed inside the tank (they can have their oil or share it), while the second is usually welded to the tank [33]. In Europe, resistive-type tap-changers are generally used.



**Figure 9.** On-load tap-changer. (a) tap-changer device commercially available; (b) diagram of the tap-changer working principle.

The tap-changer comprises a “switch” switching component and a “plug selector” selection component, as illustrated in Figure 9b. The entire switching process is driven by a single-phase induction motor placed outside the transformer.

Variation of the number of turns ratio is intended to be carried out without interrupting the load current. The process always occurs by connecting the next socket before undoing the previous connection. To avoid the high current coming from the short circuit between turns, a transition impedance is inserted in the form of electrical resistance or reactance, thus transferring the load current from one socket to the other.

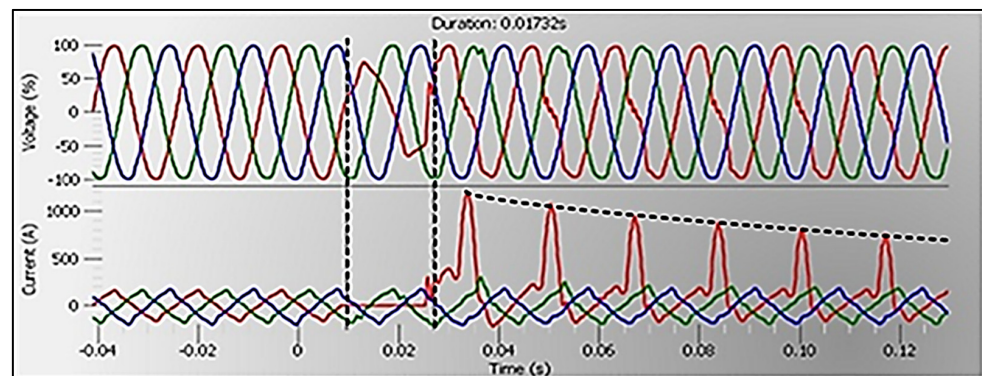
In the on-load voltage regulator, abnormal operating conditions may also arise, which will be reflected in the operation of the transformer. Some of them are presented below.

1. The lack of maintenance of this equipment can lead to a desynchronization between the selector and the tap-changer, causing the voltage regulator not to be in the correct position [34,35];
2. Old or burnt condensers in the induction motor can lead to a loss of control in the direction of governor movement or even cause the governor motor to stop and make it impossible to change the number of turns ratio;
3. With frequent use, commutator springs lose elasticity and may even break. In this case, it will not be possible to change the ratio of the number of turns of the regulator [36];
4. The voltage regulator is frequently used, which leads to wear of the entire switching mechanism [24], especially in the contacts responsible for the transition of plugs, which are subject to electric arcs. In the on-load voltage regulator, the current interruption leads to the appearance of an electric arc, which leads to the formation of gases that are the same as those that appear in the main transformer tank due to dielectric failures. As such, if the tank is shared, false conclusions about dielectric failures and their location can result;
5. When operating on the same contact for a long time, there is a risk of deposition of carbon particles, which can char due to the heat from the increased contact resistance. In extreme cases, as shown in Figure 10a, the contacts’ carbonization leads to the impos-

sibility of operation as the contacts are stuck [37]. This anomaly is not very common in on-load voltage regulators and is more relevant for no-load voltage regulators.



(a)



(b)

**Figure 10.** Abnormal condition in the on-load tap-changer (a) and current and voltage signals at the transformer terminals (b) [37].

The example illustrated in Figure 10a occurred in a substation transformer and showed the occurrence of a severe failure in the regulator switch. As can be seen from the evolution of voltages and currents at the transformer terminals in Figure 10b, the fault was reflected in the signals by the appearance of oscillations in one of the currents and the deformation associated with the respective voltage.

### 2.3.3. Tank

The tank contains the oil and provides physical protection and support for the different components of the transformer, besides ensuring the grounding of the magnetic circuit and the various metal parts. The tank may show cracks [38], essentially resulting from environmental wear and tear, such as those resulting from corrosive environments, high humidity, vibrations, and solar radiation. The tank walls may also rupture due to high-pressure gases resulting from internal arcs that vaporize the oil [39].

### 2.3.4. Cooling System

In a large power transformer, cooling is achieved through the forced circulation of oil, water, or air. Forced circulation is based on the use of pumps and fans. There is a coding depending on the internal and external cooling medium and the type of circulation they are subject to. For example, ONAN is interpreted as having an internal cooling medium of mineral oil and external air, and the circulation in both is characterized by being natural. Generally, internal cooling uses mineral oil “O” forced through the radiators and directed

from these to the “D” windings, or even if it is just forced “F”. External cooling uses “A” air or “W” water. For external circulation, there is “N” for natural air convection and “F” for forced circulation. The same transformer can have several types of cooling. Depending on the temperature and/or power it is subject to, it can activate or deactivate the fans and/or pumps [40,41].

The most significant anomalies in the cooling system lead to an increase in the temperature of the transformer oil, which affects different components of the transformer and can even lead to an increase in the pressure of the gases that form, leading to its explosion [42]. These failures can, for example, originate from cracks in the tubes where the oil circulates (causes a reduction in the amount of oil and leading to a reduction in heat exchange), or even due to anomalies in the fans due to wrong measurements of the thermometers or malfunction of the ventilation and pumping system. The example from [43] in Figure 11 makes it possible to visualize a case in which the oil level dropped and prevented its circulation since the radiator valves are at a lower level.

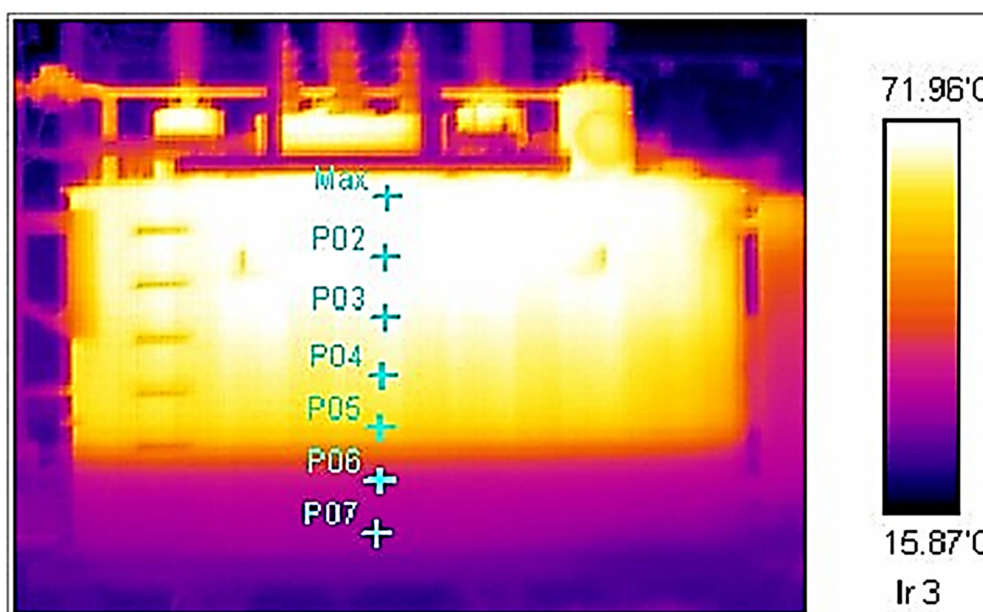


Figure 11. Transformer thermographic photograph [43].

Until now, we pointed out various abnormal operating conditions that lead to transformer failure. However, it is not straightforward to enumerate them all. Hence, we decided to outline the most frequent anomalies associated with each transformer system element. Table 1 summarizes, based on the information presented above and in [44,45], the failure modes and most recurrent causes that appear in each component.

Table 1. Failure modes and common causes are associated with the most important transformers’ components.

Component	Failure Mode	Event	Cause
Core	Loss of efficiency	Blade displacement	—Eddy currents
Windings	Short-circuit	Mechanical damage	—Manufacturing deficiencies —Corrosion —Bad maintenance —Vibrations —Mechanical displacements
		Insulation Failure	—Overvoltage —Overheating

**Table 1.** *Cont.*

Component	Failure Mode	Event	Cause
Solid insulation	Cannot provide insulation	Mechanical damage	—Cellulose aging
		Insulation Failure	—Cellulose Aging —Overheating
Insulation fluids	Short-circuit	Conductive particles in the oil	—Aging —Overheating
	Overheating	Oil does not cool	—Pumps/Fans failure —Particles in oil (aging and overheating)
Bushings	Overheating	Partial discharges and loss of dielectric properties	—Insulator contamination —Water inlet —Aging
On-load voltage regulator	Inability to change the number of turns ratio	Mechanical damage	—Breakage of springs —Lack of maintenance —Old or burnt condensers —Carbonization —Switching system wear
Oil tank	Oil leakage	Damage to tank walls	—High gas pressure —Environmental wear
Cooling system	Overheating	Cooling incapacity	—Pipe cracks —Particles in oil (aging and overheating) —Pump/fan failures

### 3. Traditional Diagnostic Methods

A faulty transformer can lead to situations that are sometimes significant in terms of their financial, technical, and environmental consequences. Hence, the need to detect and identify the fault as soon as possible.

As the price of a large power transformer is very high, a simple oil analysis can be enough to avoid costly damage associated with a prolonged interruption of its operation. Hence, it will be preferable to follow the evolution and trends deduced from the information inferred from the analysis carried out on the oil.

The analysis of gases dissolved in oil by itself is quite incomplete. Faults pointed out by the various existing methods can have different origins, giving rise to different failures. Based on [46–48], Table 2 summarizes at a macro level the four major types of failures detected by analyzing the gases dissolved in the oil and the potential reasons for them. However, to accurately determine the source of a failure, it is essential to complement the analysis of gases dissolved in oil with other existing diagnostic methods, as discussed later.

**Table 2.** Major failures in large power transformers with signatures were detected by analyzing the gases dissolved in the oil (data available in [46–48]).

Cause	Failure			
	Paper Overheating	Oil Overheating	High Energy Electrical Discharge	Low Energy Electrical Discharge
Short circuit between turns of the windings	X		X	
Winding open circuit	X		X	
Internal LTC Operation			X	
Deformation or displacement of windings	X			X

Table 2. Cont.

Cause	Failure			
	Paper Overheating	Oil Overheating	High Energy Electrical Discharge	Low Energy Electrical Discharge
Loss of connection of the crossing terminals	X		X	X
Water or too much moisture in the oil			X	X
Metallic particles in the oil			X	X
Displacement of spacers				X
Overload	X			
Insulation between blades damaged		X		
Rust or other core damage		X		
Obstacles to the passage of oil		X		
Cooling system malfunction		X		

### 3.1. Dissolved Gas-in-Oil Analysis

Transformer diagnosis through analyzing gases dissolved in oil, which fits into the philosophy of conditional maintenance, is a very effective preventive monitoring tool. It allows predictions for the status and initial defects that may appear during transformer operation. It is an essential technique in determining the transformer's "health status".

The two main causes of the formation of those gases are *electrical disturbances* and *thermal decomposition*. The rate at which each gas is produced depends on the material's temperature and volume. Transformer failure diagnosis has 8 key gases: hydrogen ( $H_2$ ), methane ( $CH_4$ ), ethane ( $C_2H_6$ ), ethylene ( $C_2H_4$ ), acetylene ( $C_2H_2$ ), carbon monoxide (CO), and carbon dioxide ( $CO_2$ ).

Failures detected by analyzing those gases are thermal failures, electrical discharges (low and high energy), and partial discharges. Thermal failures result from an excessive rise in insulation temperature and can occur in paper or oil. Oil's thermal failures are divided into several classes since, depending on the temperature, the gases formed differ. Here, *low- or high-energy electrical discharges* refer to insulation disruptions between conductors [49,50].

In Table 3, we present a color scale representing the association between the concentration rate of each gas and each type of failure occurring in the transformer. The table presented was constructed based on information collected from references [51–53]. The colors symbolize the different quantities of gases produced, with green being associated with small quantities (trace), yellow with medium quantities, and red with large quantities.

The total concentrations of the gases, their relative proportions, and the rate of increase of each gas makes it possible to assess the condition of the transformer. Several criteria allow associating these parameters with the type of failure that occurred, the most common currently being the method of Rogers, Doernenburg [54], IEC 60,599 [54], Duval [55], Key Gas [55], and TDCG [56]. These criteria are empirical, and the results are based on the correlation between the detected gases. Many use ratios to determine the failure, which makes it possible to eliminate the oil volume effect and some sampling effects [57]. Below are some of the most used ratios and possible types of failure associated with [56,57]. Note that these are only significant and should only be calculated if at least one of the gases exceeds its typical concentration and growth rate value.

R1: ( $CH_4/H_2$ )—Partial Discharges

R2: ( $C_2H_2/C_2H_4$ )—Arc-electric

R3: ( $C_2H_2/C_2H_4$ )

R4: ( $C_2H_6/C_2H_2$ )—High-intensity discharge

R5: ( $C_2H_4/C_2H_6$ )—Oil overheating  $> 500\text{ }^\circ\text{C}$

R6: (CO<sub>2</sub>/CO)—Cellulose overheating

R7: (N<sub>2</sub>/O<sub>2</sub>)—Oxygen consumption; sealing defect

Below, we briefly describe each method and its main characteristics.

**Table 3.** Standardization regarding gases produced in the transformer and associated failures.

Failure	H <sub>2</sub>	CH <sub>4</sub>	C <sub>2</sub> H <sub>6</sub>	C <sub>2</sub> H <sub>4</sub>	C <sub>2</sub> H <sub>2</sub>	CO	CO <sub>2</sub>
Thermal paper							
Thermal oil (150–300 °C)							
Thermal oil (300–700 °C)							
Thermal oil (>700 °C)							
Low energy discharge							
High energy discharge (Arc-electric)							
Partial discharge							

### 3.1.1. IEC 60,599 Method

This method classifies the anomalies according to Table 4. The ratios must be observed when one or more gases have high concentrations or growth. The input variables are the ratios R2, R5, and R1, and, instead of R1, you can also use C<sub>2</sub>H<sub>2</sub>/C<sub>2</sub>H<sub>6</sub> [54].

**Table 4.** IEC method—Failures and the correspondent ratio limits (adapted from [54]).

Abbreviation	Failure	R2 (C <sub>2</sub> H <sub>2</sub> /C <sub>2</sub> H <sub>4</sub> )	R1 (CH <sub>4</sub> /H <sub>2</sub> ) ou C <sub>2</sub> H <sub>2</sub> /C <sub>2</sub> H <sub>6</sub>	R5 (C <sub>2</sub> H <sub>4</sub> /C <sub>2</sub> H <sub>6</sub> )
PD	Partial Discharges	Negligible value	R < 0.1	R < 0.2
D1	Low Energy Discharges	1.0 < R	0.1 < R < 0.5	1.0 < R
D2	High Energy Discharges	0.6 < R < 2.5	0.1 < R < 1.0	2.0 < R
T1	Thermal Failure T < 300 °C	Negligible value	Negligible value	1.0 < R
T2	Thermal Failure 300 °C < T < 700 °C	R < 0.1	1.0 < R	1.0 < R < 4.0
T3	Thermal Failure T < 700 °C	R < 0.2	1.0 < R	4.0 < R

### 3.1.2. Duval Method

Duval's method interprets dissolved gases through a triangle of relative percentages of CH<sub>4</sub>, C<sub>2</sub>H<sub>2</sub>, and C<sub>2</sub>H<sub>4</sub> gases. The triangle is shown in Figure 12, where the different colored regions are associated with different faults. The relative percentage of each gas is obtained by dividing the quantity (in ppm) of the gas by the sum of the quantities of the three gases [58]. For example, to get the relative percentage of CH<sub>4</sub>:

$$\%CH_4 = \frac{CH_4}{CH_4 + C_2H_2 + C_2H_4} \quad (1)$$

where  $\text{CH}_4$ ,  $\text{C}_2\text{H}_2$ , and  $\text{C}_2\text{H}_4$  represent the amounts of the respective gases in ppm.

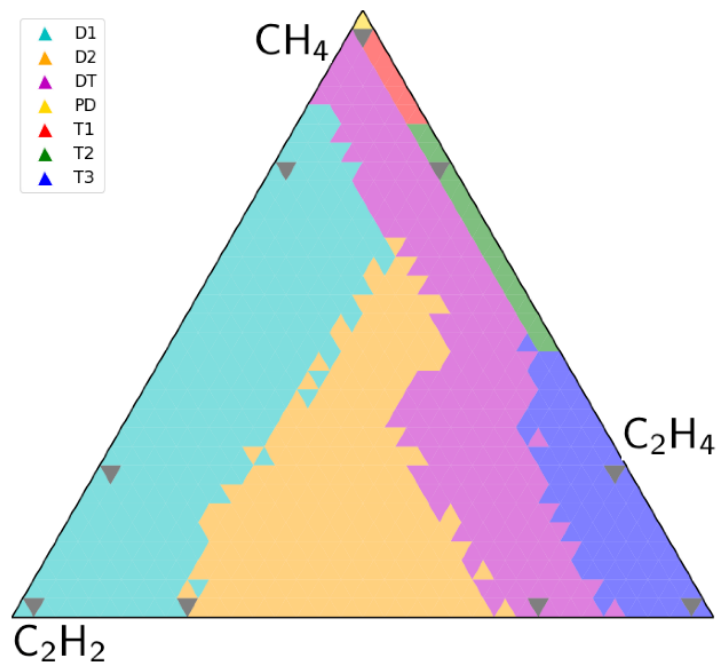


**Figure 12.** Duval's triangle and associated faults. Adapted from [49], licensed under CC BY 4.0.

### 3.1.3. Key Gas Method

The faults are qualitatively determined by the concentration of the key gases (in ppm) based on the typical or predominant gases at various temperatures. In Table 5, the classification of the types of failures according to the associated key gases is presented [54].

**Table 5.** Key Gas Method—Key gases and associated failures (adapted from [54]).

Key Gases	Failures	Typical Emission Proportion
$\text{H}_2$ and $\text{C}_2\text{H}_2$	High energy electrical discharge	Large amounts of $\text{H}_2$ and $\text{C}_2\text{H}_2$ . Small quantities of $\text{CH}_4$ and $\text{C}_2\text{H}_4$ . The formation of $\text{CO}_2$ e $\text{CO}$ indicates paper combustion.
$\text{C}_2\text{H}_4$	Oil overheating	Mainly $\text{C}_2\text{H}_4$ . Reduced quantities of $\text{C}_2\text{H}_6$ , $\text{CH}_4$ , and $\text{H}_2$ . Residues of $\text{C}_2\text{H}_2$ , with large temperature failures.
$\text{CO}$	Paper overheating	Mainly $\text{CO}$ and $\text{CO}_2$ .
$\text{H}_2$	Electrolysis	Mainly $\text{H}_2$ .
$\text{H}_2$	High energy electrical discharge, partial discharge	Mainly $\text{H}_2$ . Small amounts of $\text{CH}_4$ . Trace elements of $\text{C}_2\text{H}_4$ and $\text{C}_2\text{H}_6$ .

### 3.1.4. Doernenburg's Method

This method suggests three types of faults: thermal, electric arc, and low-energy discharge (corona). This method only considers its use when the concentrations of  $\text{H}_2$ ,  $\text{CH}_4$ ,  $\text{C}_2\text{H}_2$ , and  $\text{C}_2\text{H}_4$  exceed twice the established limits and the concentrations of  $\text{CO}$  and  $\text{C}_2\text{H}_6$  gases exceed three times the established limits. However, the method is complex and often leads to "none interpretation" [54]. The authors present a flowchart of the procedure to be carried out to obtain the transformer diagnosis. A gas concentration limit ( $L_1$ ) is specified for each of the gases. This  $L_1$  limit is shown in Table 6, enough for one of the gases to exceed the limit to advance.

**Table 6.** Limit  $L_1$  specified for each gas and its values that cannot be exceeded.

Gases	Limit $L_1$ (ppm)
H <sub>2</sub>	100
CH <sub>4</sub>	120
CO	350
C <sub>2</sub> H <sub>2</sub>	35
C <sub>2</sub> H <sub>4</sub>	50
C <sub>2</sub> H <sub>6</sub>	65

### 3.1.5. TDCG Method (“Total Dissolved Combustible Gas”)

This methodology is present in North America’s history, as it had its initial application as an important tool in analyzing gases in mines [48]. It does not offer a diagnosis related to transformer failures. However, it is relevant in indicating the variation of gas levels. In ppm, the TDCG value is obtained from H<sub>2</sub>, CH<sub>4</sub>, C<sub>2</sub>H<sub>2</sub>, C<sub>2</sub>H<sub>4</sub>, C<sub>2</sub>H<sub>6</sub>, and CO gases, computing the augmenting rate by making the difference between the TDCG values of two samples divided by the time (days) between samples. The TDCG limits, sample intervals, and suggested operating procedures are presented in Table 7.

**Table 7.** TDCG Method—Limits and operating procedures (adapted from [55]).

TDCG Level (ppm)	TDCG Generation Rates (ppm/Day)	Sampling Intervals and Operating Actions for Gas Generation Rates	
		Sampling Interval	Operating Procedures
<720	<10	Twice a year	Continue normal operation.
	10–30	Quarterly	
	>30	Monthly	Caution is necessary. Analyze individual gases to find the cause. Determine load dependence.
721–1920	<10	Quarterly	Caution is extremely necessary. Analyze individual gases to find the cause. Determine load dependence.
	10–30	Monthly	
	>30	Monthly	
1921–4630	<10	Monthly	Exercise extreme caution. Analyze individual gases to find the cause. Plan outage.
	10–30	Weekly	
	>30	Weekly	
>4630	<10	Weekly	Exercise extreme caution. Analyze individual gases to find the cause. Plan outage.
	10–30	Daily	
	>30	Daily	Consider removal from service.

### 3.1.6. CO<sub>2</sub>/CO Ratio

The CO<sub>2</sub>/CO ratio is usually used as an indicator of the thermal decomposition of cellulose, and only for ratio values lower than three should this indication be taken into account [49].

### 3.1.7. Rogers Method

A simple method of diagnosing transformer faults. Its validity is based on the correlation of the results of many failures identified with the analysis of the gases in each case. Table 8 summarizes how the associated faults are attributed according to the values of the ratios chosen in this method.

**Table 8.** Rogers Method—Relationship between ratios and failures (adapted from [54]).

Ratio R1 (CH <sub>4</sub> /H <sub>2</sub> )	Ratio R2 (C <sub>2</sub> H <sub>2</sub> /C <sub>2</sub> H <sub>4</sub> )	Ratio R5 (C <sub>2</sub> H <sub>4</sub> /C <sub>2</sub> H <sub>6</sub> )	Failure
0.1 < R < 1.0	R < 0.1	R < 1.0	Normal operation.
R < 0.1	R < 0.1	R < 1.0	Low energy electrical discharge
0.1 < R < 1.0	1.0 < R < 3.0	3.0 > R	High-energy electrical discharge
0.1 < R < 1.0	R < 0.1	1.0 < R < 3.0	Low temperature thermal failure
1.0 > R	R < 0.1	1.0 < R < 3.0	Thermal failure <700 °C
1.0 > R	R < 0.1	3.0 > R	Thermal failure >700 °C

### 3.2. Oil Quality

Several tests are carried out on the oil to verify its contamination, deterioration status, and electrical properties. Electrical, physical, and chemical tests (dielectric strength, power factor, interfacial tension, color, sludge and sediment, acidity index, relative humidity, kinematic viscosity, and particle content, among others). Table 9 presents some of the methods and standards for each of the most important tests [59].

**Table 9.** Oil quality tests and standards/methods. Adapted from [59], licensed under CC BY 4.0.

Test	Standard/ ASTM Method	IEC
Color	ASTM D1500	ISSO 2049
Interfacial Tension	ASTM D971	ISSO 6295
Visual inspection	ASTM D1524	-
Breakdown voltage	ASTM D1816	IEC60156
Dissipation factor	ASTM D924	IEC247
Neutralizing number	ASTM D664	IEC62021
Water content	ASTM D1533	IEC60814

#### 3.2.1. Color

This test allows you to gain insight into the oil's state quickly. The evaluation is compared with normalized standards, assigning an oil color number. Rapid color changes or high numbers are associated with advanced aging and/or oil contamination [60].

#### 3.2.2. Interfacial Tension

The interfacial tension value, which determines the tension at the interface between two liquids (oil and water), indicates soluble polar contaminants in the oil [60].

#### 3.2.3. Dielectric Breakdown Voltage

The dielectric breakdown voltage measures the oil's ability to withstand electrical voltages. The test is carried out by immersing two electrodes in oil at a distance, as shown in Figure 13. Subsequently, several levels of alternating voltage are applied until the break occurs. Contaminants such as water, sediment, and conductive particles reduce the breakdown voltage level [60].



**Figure 13.** Dielectric breakdown voltage measurement test [57].

#### 3.2.4. Dissipation Factor

The dissipation factor measures the loss angle ( $\tan \delta$ ) and indicates the leakage current flowing through the oil. With the deterioration or contamination of the oil, the value of the loss angle increases, and, for new oils, it is expected to obtain typical values lower than 0.005 [60].

#### 3.2.5. Neutralizing Number

The neutralizer number or acidity value is an indicator of the oxidation/decomposition of the oil. However, acids in the oil can also arise from outside sources, such as a polluted atmosphere. These acids, together with water, can lead to corrosion inside the transformer [60].

#### 3.2.6. Water Content

The water content is a very important parameter to control, as it accelerates the insulation aging process and, at the same time, is one of the products resulting from this process. A more detailed explanation of this test and its importance is given in Section 4.3.

#### 3.2.7. Limits

Table 10 presents the limits suggested in [61] for some of the tests carried out to determine the quality of transformer oil.

**Table 10.** Transformer oil quality tests and their limits.

Test	Value According to Voltage Classes		
	$\leq 69$ kV	69–230 kV	$\geq 230$ kV
Dielectric breakdown voltage [kV] for 1mm electrode distance (minimum value)	23	28	30
Interfacial tension [mN/m] (minimum value)	25	30	32
Neutralizing number [mg KOH/g] (maximum value)	0.2	0.15	0.1
Water content [ppm] (maximum value)	35	25	20

### 3.3. Degree of Polymerization

The degree of polymerization is defined as the number of glucose rings in a cellulose macromolecule (Figure 14). It provides an indication of the paper's state and the insulation system's mechanical stress. This can be measured indirectly through the furanic compound's analysis or paper samples.

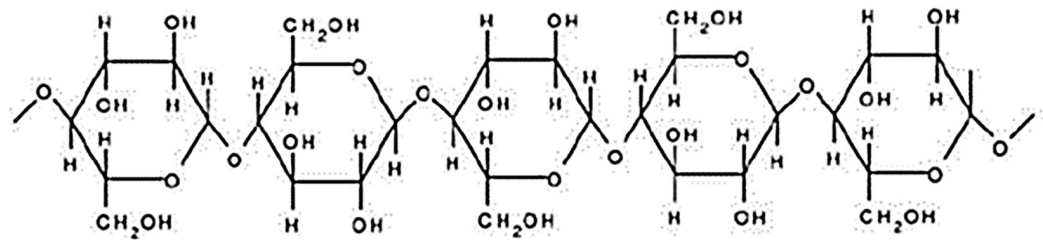


Figure 14. Chemical structure of cellulose molecule [9].

The degree of polymerization is defined as the number of glucose rings in a cellulose macromolecule. It indicates the paper's condition and the mechanical strength of the insulation system. This can be measured indirectly via an analysis of furan compounds or paper samples. The Arrhenius Equation (2) estimates the degree of polymerization ( $DP$ ) at a given time  $t$  after its initial measurement. It depends on activation energy ( $E_a$ ), chemical environment ( $A$ ), hotspot temperature ( $T$ ), and gas constant ( $R$ ).

$$\frac{1}{DP(t)} - \frac{1}{DP(0)} = A \cdot e^{-\frac{E_a}{R \cdot T}} \cdot t = kt \quad (2)$$

where

$DP(t)$  and  $DP(0)$  correspond to the  $DP$  at time  $t$  and start, respectively.

$A$ —constant that depends on the chemical environment.

$E_a$ —activation energy of the reaction in kJ/mol

$R$ —perfect gas constant (8314 J/mol/K)

$T$ —the absolute temperature in K

$k$ —speed constant (aging)

### 3.3.1. Analysis of Furanic Compounds

Furanic compounds are a group of organic components formed by the deterioration of cellulose material (paper) in the transformer. Overheating with moisture and oxidation accelerates paper deterioration, resulting in furanic compounds that dissolve in the oil. An analysis by high-pressure, high-resolution liquid chromatography indirectly characterizes the degree of cellulose polymerization.

The value of the degree of polymerization obtained through the analysis of furanic compounds refers to the average value of the entire solid insulation structure. As paper does not age uniformly, there may be regions where degradation is more severe. As described above, the high  $\text{CO}_2$  and  $\text{CO}$  levels indicate the need to analyze furanic compounds. The five main types of furanic compounds that can form are:

- (a) 2-furfuraldehyde (2FAL)
- (b) 2-acetylfuran(2ACF)
- (c) 2-furfuryl alcohol (2FOL)
- (d) 5-methyl-2-furfuraldehyde (5MEF)
- (e) 5-hydroxy-methyl-2-furfuraldehyde (5HMF)

The measurement of furanic compounds in mineral oil is carried out following the IEC 61198 standard. Several methods relate the degree of polymerization with furanic compounds found in the oil. We highlight the *Chendong* method [54] (Equation (3)) applicable to transformers with kraft paper, the *Stebbins* method (Equation (4)) [54], which results from a modification of the *Chendong* method for transformers with thermally improved paper, the *De Pablo* method (Equation (5)) [56] which was developed based on the theory of cellulose chain splitting and the *Pahlavanpour* method (Equation (6)) [62], which is a modification of the *De Pablo* method where it is considered that the aging of the paper is not uniform. It is assumed that 20% of the inner layers near the winding degrade at twice

the speed, which associates the degree of polymerization with the concentration of furanic compound 2FAL [62].

$$\text{Chendong :} \quad DP = \frac{1.51 - \log\left([2FAL]_{ppm}\right)}{0.0035} \quad (3)$$

$$\text{Stebbins :} \quad DP = \frac{1.655 - \log\left([2FAL]_{ppm}\right)}{0.0035} \quad (4)$$

$$\text{DePablo :} \quad DP = \frac{7100}{8.8 + [2FAL]_{ppm}} \quad (5)$$

$$\text{Pahlavanpour :} \quad DP = \frac{7100}{8.8 + [2FAL]_{ppm}} \quad (6)$$

### 3.3.2. Direct Measurement through Paper Samples

To directly determine the degree of polymerization, a paper sample is required. However, it is necessary to take the transformer out of service. The value is obtained by viscosimetric measurement according to the IEC 60450 standard. Once again, the value obtained cannot be generalized for the entire winding.

### 3.4. Frequency Response Analysis

By analyzing the transformer's frequency response, it is possible to detect any deformations in the windings by comparison with a previously obtained frequency response reference. Differences in resonance frequency or magnitude are related to changes in inductances and capacities, which are defined according to the physical dimensions and materials of the transformer. This frequency response is obtained by imposing a voltage pulse at the transformer's input and measuring the frequency spectrum of its response at the output obtained by the Fourier Transform. This method, however, requires taking the transformer out of service. However, there are currently attempts to carry out this test in service, in which electrical transients that already exist in the electrical network are used. This measurement is currently simple to perform. However, the interpretation of the results is a little complicated, and a consensus is often not reached [4,41].

### 3.5. Power Factor

The power factor or loss factor is an important measure in monitoring the condition of the transformer and crossovers. The power factor refers to the quotient between the leakage current of the resistive component and the capacitive component, which result from the application of an alternating voltage. If the insulation were perfect, the capacitive component of the current would naturally be in advance of 90° relative to the voltage. However, as there are Joule losses, this advance is less than 90°, as the resistive component increases with the deterioration of the dielectric. This test is done to determine the insulation condition between windings and compartments, and it only indicates the general state of the insulation system [47].

### 3.6. Excitation Current

The measurement of the excitation current, performing a no-load test, allows the identification of faults in the magnetic circuit and the windings of single-phase or three-phase transformers, such as short-circuited windings open-circuit problems in the voltage regulator, and also, failures in the electrical connections. When any of these problems occur, the reluctance of the magnetic circuit changes, which affects the current needed to impose a magnetic flux on the core. Test results should be compared with previous tests or other phases (in the three-phase) [4].

### 3.7. Leakage Reactance

Also called short-circuit testing, leakage inductance measurement is a traditional method to detect changes in winding geometry and the core. These deformations alter the magnetic flux and, consequently, the leakage inductance. The values obtained are compared with information from the nameplate, previous tests, or similar transformers [4].

### 3.8. Electrical Insulation Resistance

This test is usual. However, it is not standardized due to the variability of results depending on the environment at the time of measurement (temperature, humidity, level of impurities in the insulation materials). The electrical insulation resistance provides information about its state [4].

### 3.9. Electrical Resistance of Windings

The electrical resistance of each winding is measured in direct current. It is necessary to measure and record the temperature associated with each resistance measurement, as the temperature varies with the resistance. This test indicates the status of the windings and the voltage switch. A variation of more than 5% concerning the information on the nameplate indicates serious damage to the conductor [4].

### 3.10. Partial Electrical Discharges

The partial discharge test is essentially qualitative. Partial discharges result from local dielectric disruptions in the insulation system. The intensity and frequency of partial discharges are a good indicator of the state of the insulator, as they increase along with the corrosion and decomposition of the insulating material. Partial discharges generate electromagnetic waves, acoustic waves, local overheating, and chemical reactions. To understand its location, both acoustic and electrical signals must be measured. There is already some continuous monitoring equipment based on the measurement of these two variables [48].

### 3.11. Relationship between Turns

Coils are subject to electrical and mechanical wear, which can cause short circuits or open circuits. The ratio of the number of turns ( $N_2/N_1$ ) is related to the quotient between the secondary voltage ( $V_2$ ) and the primary voltage ( $V_1$ ), that is,  $V_2/V_1 \approx N_2/N_1$ . The value of the ratio between turns must not deviate more than 0.5% from the ratio between the nominal voltages of the windings stipulated on the nameplate.

### 3.12. Return Voltage and Polarization Currents

The restoration voltage method allows access to the water content and insulation system's degradation level. This test is carried out by charging the insulator's dielectric structure with electrical charges by applying a voltage pulse, then creating a short-circuit through an external impedance. The signal obtained when removing the external impedance allows for characterizing the insulation system's state. By analyzing the frequency response of the polarization and depolarization currents, it is also possible to perceive the condition of the insulating material [4].

### 3.13. Mechanical Vibrations

Transformer vibrations originate in the core, induced by magnetostriction (change in the shape of the ferromagnetic material due to a change in the magnetic field which leads to core vibration), and vibrations in the windings, induced by electromagnetic forces (interaction force between the current of the windings and the dispersion field, resulting in its vibration of the windings). The excitation frequency of the core and windings is twice the frequency of the alternating current, as the forces vary with the square of the voltage and the current of the electrical signal, respectively. It is also known that the core

presents vibration frequencies of greater magnitude due to the non-linearities of the core's magnetostriction.

Sensors (accelerometers) are installed on the sides and top of the transformer tank to measure these vibrations. Several sensors are placed to reduce uncertainty due to the dimensions and complexity of the transformers. The signals are generally transmitted through an optical cable and registered in a specific device. With these signals, it is then possible to detect the condition of the windings and the magnetic circuit [49].

### 3.14. Temperature

The load capacity of transformers is limited by the temperature of the windings (which is not uniform). The traditional method for estimating windings temperature is to measure the temperature at the top and bottom of the tub. The real limiting factor is the "hot spot" located on top of the transformer that is not directly accessible. Sensors have been developed to directly measure the temperature of the "hot spot" of the windings, the most reliable of which seem to be fiber optics. These sensors are placed on the spacers or the conductors to be monitored. The hot spot temperature, according to IEC, must not exceed 98 °C [48].

### 3.15. Infra-Red Test

Direct monitoring via thermographic images obtained by infrared testing is important to prevent abnormal operating conditions and protect the insulation material. The high temperatures in the transformer, especially the "hot spot," contribute to oil decomposition, paper deterioration, and power losses. With this test, it is possible to locate the hot zones at a temperature higher than the external surface of the transformer. Four colors are displayed in the thermal image: white, red, blue, and black. Warmer zones appear in white and red colors, and cooler zones in black and blue [41].

### 3.16. Bushings Condition

Transformer bushings are one of the most frequent causes of breakdowns, and in most cases, the breakdowns result from water ingress. Those in contact with the outside suffer greater deterioration and are more vulnerable to external accidents. The techniques used to monitor the transformer bushings are adaptations of the abovementioned techniques (analysis of gases dissolved in oil, oil quality, partial discharges, infrared thermography, power factor, temperature, etc.) [4].

### 3.17. Tap-Changer Condition

The transformer's voltage regulator can focus on various abnormal operating conditions. Adding to this, the voltage regulator is one of the few transformer elements that perform mechanical movements. It is subject to greater wear. As such, monitoring this type of apparatus is essential. The monitoring and analysis of the temperature in the resistance of the motor windings of the power supply that drives the commutator, the gases dissolved in the oil, and its vibration pattern stand out [4].

## 4. Online Diagnostic Models for Power Transformers

After reviewing the diagnostic methodologies of power transformers, it is interesting to understand which ones have monitoring applications automatically and continuously over time and how they can be applied. Monitoring is done through multiple sensors that capture some variables that make it possible to determine the status of the transformer and its components.

Continuous monitoring overtime automatically allows companies that have transformers to monitor the status of their assets "minute-by-minute," as such, it allows early detection of anomalies, preventing them from evolving into situations with large technical and economic losses.

#### 4.1. Thermal Model

It is essential to monitor the temperature of the transformer, especially the hotspot, which is somewhere on the top of the transformer, as shown in Figure 15, to increase operating efficiency and reduce the probability of transformer shutdown. Another important measure of temperature is the top oil, which represents the temperature at the top of the transformer oil. It is possible to obtain the hot spot temperature directly, through a fiber optic system, or indirectly, through models that estimate it.

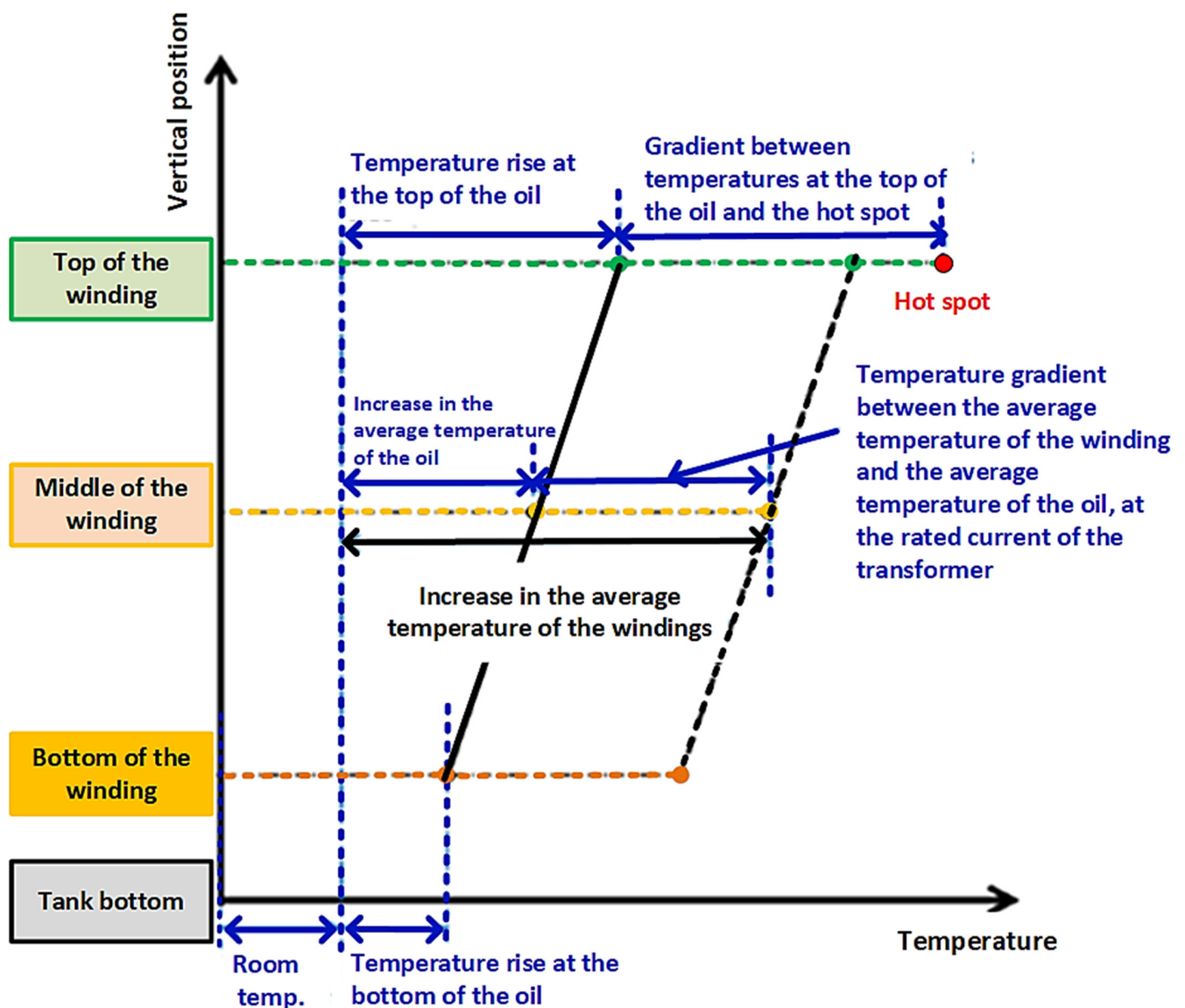


Figure 15. Diagram for the thermal model of the power transformer. Adapted from [63], licensed under CC BY 4.0.

The calculation of the hot spot temperature, according to [63], is essentially based on the diagram in Figure 15, which is based on the following hypotheses:

1. The oil temperature in the transformer tank increases linearly between the bottom and the top, regardless of the type of cooling;
2. The temperature along the winding also increases linearly between the bottom and the top, regardless of the type of cooling. For the same horizontal position, this temperature always exceeds that of the oil by the value of a constant  $gr$  (gradient between the average temperature of the windings and the oil);

3. The temperature rise of the hot spot is greater than the temperature rise of the winding on top of the winding. The difference is determined by multiplying the constant  $gr$  by the hot spot factor (HSF).

In [50], it is indicated that it is possible to estimate the temperature at the top of the oil ( $\theta_0$ ) through Equation (7), which depends on the ambient temperature ( $\theta_a$ ), the load factor ( $K$ ), which is calculated by dividing the rms value of the current at its nominal value, the ratio between the load losses at the nominal current and the no-load losses ( $R$ ), the exponent of the total losses versus the increase in temperature at the top of the oil ( $x$ ), the increase in steady-state temperature under nominal loss conditions ( $\Delta\theta_{or}$ ), the average of the oil's thermal time constants ( $\tau_0$ ) and the thermal model constant ( $k_{11}$ ).

$$\left[ \frac{1 + K^2 \cdot R}{1 + R} \right]^x \cdot (\Delta\theta_{or}) = k_{11} \cdot \tau_0 \cdot \frac{d\theta_0}{dt} + [\theta_0 - \theta_a] \quad (7)$$

To obtain the hot-spot temperature ( $\theta_h$ ), it is necessary to add to the top oil temperature ( $\theta_0$ ) the gradient between the hot-spot temperature and the top oil temperature with the considered load ( $\Delta\theta_h$ ). To facilitate the calculation of this gradient, it is divided into two differential Equations (8) and (9), and then the resulting gradients,  $\Delta\theta_{h1}$  and  $\Delta\theta_{h2}$  (Equation (10)), is added.

$$\Delta\theta_h = \Delta\theta_{h1} - \Delta\theta_{h2} \quad (8)$$

$$k_{21} \cdot K^y \cdot (\Delta\theta_{hr}) = k_{22} \cdot \tau_w \cdot \frac{d\Delta\theta_{h1}}{dt} + \Delta\theta_{h1} \quad (9)$$

$$(k_{21} - 1) \cdot K^y \cdot (\Delta\theta_{hr}) = \frac{\tau_0}{k_{22}} \cdot \frac{d\Delta\theta_{h2}}{dt} + \Delta\theta_{h2} \quad (10)$$

The remaining symbols of variables or parameters that appear in these three equations are the thermal model constants ( $k_{21}$  and  $k_{22}$ ), the winding time constant ( $\tau_w$ ) and the current exponent versus the winding temperature rise ( $y$ ).

The maximum oil top temperature for normal charge cycles is 105°C, and the hot spot temperature is 120 °C. The standard also suggests values for the power transformer's characteristic parameters according to the cooling type presented in Table 11 [50].

**Table 11.** Transformer oil quality tests and their limits for different cooling methods.

Test Measure	ONAN ("Oil Natural Air Natural")	ONAF ("Oil Natural Air Forced")	OF <sup>(a)</sup> ("Oil Forced")	OD <sup>(b)</sup> ("Oil-Directed")
$x$	0.8	0.8	1.0	1.0
$y$	1.3	1.3	1.3	2.0
$R$	6.0	6.0	6.0	6.0
$\tau_0$ (min)	210	150	90	90
$\tau_w$ (min)	10	7	7	7
$\Delta\theta_{or}$ (K)	52	52	56	49
$\Delta\theta_{hr}$ (K)	26	26	22	29
$k_{11}$	0.5	0.5	1.0	1.0
$k_{21}$	2.0	2.0	1.3	1.0
$k_{22}$	2.0	2.0	1.0	1.0

(a) OF includes OFAN, OFAF, and OFWF cooling types. (b) OD includes ODAN, ODAF, and ODWF cooling types.

An example of calculation using the differential equations in (7), (9), and (10) is described in [50], which emphasizes the fact that the sampling time must be lower than half the time constant of the windings ( $w_e$ ), which is in the order of 7 min. Thus, the sampling period should be less than 3 min. If there is still information on the type of cooling at each

moment, the constants must correspond to this one. In other words, if the transformer is ONAN in an instant, the constants referring to this type of cooling must be used for calculation purposes. If, at another moment, the type of cooling changes to ONAF, the constants must be changed according to the table to those that correspond to ONAF cooling.

#### 4.2. Model for Estimating Water Content in Insulation (Paper and Card) and Temperature of Water Bubbles

The condition of the insulation is an essential aspect of the reliability of transformer operation, as transformers with high water content in the paper have a higher aging rate (acceleration of paper decomposition) and cannot withstand, without risk, higher loads since there is a greater possibility of bubble formation [12]. These are formed when there is an increase in temperature, causing the absorbed water to evaporate with high steam and pressure in the inner layers of the paper. If the pressure is too high, it leads to the expulsion of oil from the paper layers and the formation of bubbles on the surface of the insulation, leading to a decrease in the dielectric capacity [64].

The water in power transformers is mostly dissolved and can move between oil and solid insulation. However, some water is associated with by-products resulting from oil oxidation, which is only partially available for migration. Most water is found in solid insulation (paper and cardboard). The average water content in it is almost constant under normal conditions over time, the opposite being true for oil. An example of the water content distribution in a 25 MVA transformer [53] is presented in Table 12, in which the above is illustrated.

**Table 12.** Water distribution in a 25 MVA transformer for different temperatures.

Insulation	40 °C		80 °C	
Oil (25,000 L)	10 ppm	0.25 kg	80 ppm	2.0 kg
Paper (2500 kg)	3 %	75 kg	2.93%	73.25 kg
<b>Total</b>		<b>75.25 kg</b>		<b>75.25 kg</b>

Water appears in the transformer through three distinct sources [54]:

- Residual water that comes from manufacturing—During manufacturing, water is installed in the different components of the transformer and, despite drying, there is always a portion of water that remains, typically 0.4–1%;
- Entry from the atmosphere—The atmosphere is considered the main source of water for transformers, which can enter, for example, by exposure to humid air during installation or repairs and due to cracks that expose the inside of the transformer;
- Aging of oil and cellulose—The decomposition of cellulose, which essentially consists of breaking the bonds of glucose chains, is reflected in the appearance of water and other compounds. Oil oxidation also contributes to water formation. The normal annual water increase is approximately 0.1% [54].

##### 4.2.1. Measurement Methods

There are several ways to measure water content on paper, divided into direct and indirect. The direct measurement method extracts a paper sample and performs Karl Fischer titration [54]. To indirectly access the water content of the paper or cardboard insulation, one takes samples from the water content in oil or measures electrical quantities, such as the power factor or the dielectric response. The simplest and most common method is measuring the water content in oil. The methodology consists of three steps:

- Obtaining an oil sample from the transformer in service;
- Measurement of water content in oil (ppm) through Karl Fischer titration;
- Estimating water content in paper or board insulation (%) using equilibrium curves. Figure 16 shows an example of these curves published by Oomen in 1984 [53].

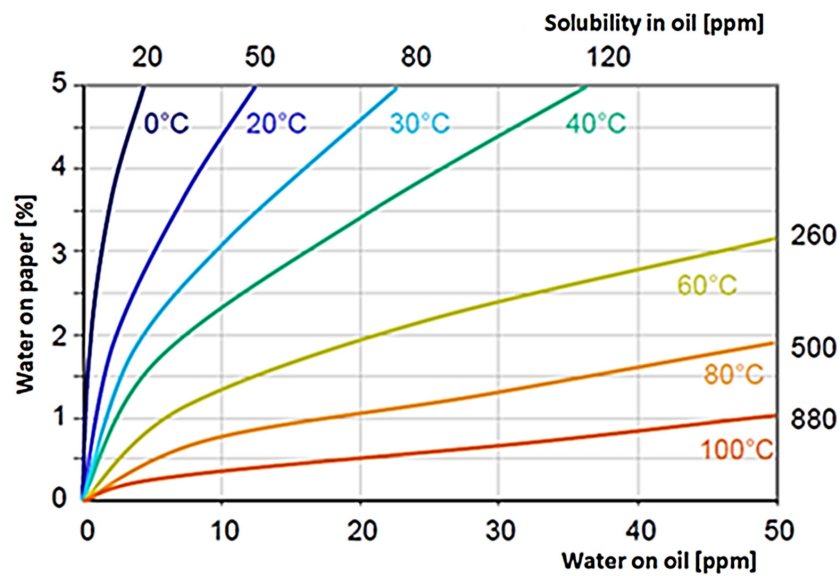


Figure 16. Oomen equilibrium curves, adapted from [54].

The applicability of these curves is subject to thermodynamic equilibrium. However, in practice, thermal stability conditions are never achieved. In addition to transformer load variations, the transformer is subjected to daily and seasonal temperature variations. Thus, balance curves cannot be directly applied. Other relevant errors are described in [54], such as: obtaining different results using different curves and different water contents along the winding due to the temperature gradient.

#### 4.2.2. Calculation of Water Content in the Paper

To estimate the water content of the paper, it is common to use the Fessler Equation (11) [53]. He combined data from Houtz, Ewart, Oomen, and their experiment [55] to obtain an equation that allows estimating the water content in the paper (WCP) through temperature (T) and water vapor pressure (p) exercised by the role.

$$WCP = 2.173 \cdot 10^{-7} \cdot p^{0.6685} \cdot e^{\frac{4725.6}{T+273.15}} \tag{11}$$

Through the definition of relative saturation (RS) [52], it is possible to associate the pressure (p) with the water-in-oil content (WCO). Equation (12) represents the relative saturation of an ideal gas or liquid and is defined as the ratio of WCO and water-in-oil solubility (WS). In contrast, Equation (12) refers to a solid and is defined as the ratio between the water vapor pressure (p) exerted by the paper and the saturation water vapor pressure (ps) [52].

$$RS = \frac{WCO}{W_S} \cdot 100\% \tag{12}$$

$$p_{cellulose} = p_{oleo} = p_{ar} \tag{13}$$

Under thermodynamic equilibrium conditions, which are obtained when thermal, mechanical, and chemical equilibrium is reached, the migration of water molecules within the materials and the migration between oil and cellulose tends to zero [52]. This corresponds to equal vapor pressure in the different materials (Equation (14)).

$$p_{cellulose} = p_{oleo} = p_{ar} \tag{14}$$

Thus, under these conditions, the relative saturation also takes the same value in different adjacent materials, as indicated in Equation (15).

$$RS_{cellulose} = RS_{oleo} = RH_{ar} \tag{15}$$

Using the equality of (15) in (12) and (13), we obtain:

$$\frac{WCO}{W_s} = \frac{p}{p_s} \quad (16)$$

The solubility of water in oil ( $W_s$ ) is calculated using Equation (17) [52].

$$W_s = 10^{-\frac{B}{T+273.15} + A} \quad (17)$$

In [24], it is suggested that B takes the value of 1567 and A the value of 7.0895. However, parameters A and B vary depending on the oil and its condition.

It is also necessary to calculate the saturation water vapor pressure to determine the water vapor pressure. In 1981, Buck [56] devised an expression for its calculation (18).

$$p_s = 0.00603 \cdot e^{\frac{17,502 \times T}{240.97 + T}} \quad (18)$$

It is concluded that the water vapor pressure is estimated by Equation (19), which results from the substitution of (17) and (18) in (16).

$$p = \frac{WCO}{10^{-\frac{B}{T+273.15} + A}} * 0.00603 * e^{\frac{17,502 \times T}{240.97 + T}} \quad (19)$$

Finally, the water content of the paper is estimated by substituting (19) for (11). This value has some inherent errors, which can be reduced by making a long-term average, thus approximating the equilibrium condition [54].

It is proved in [56] that an average of seven days offers a good accuracy of the water content in solid insulation for those seven days. That is, weekly averages are recommended. It is also suggested that by making a moving window average of the seven previous days, it is possible to obtain valid values of daily water content instead of weekly.

#### 4.2.3. Temperatures Considered in the Previous Equations

The temperatures of the equations vary, and for Equation (17), the temperature must be the temperature at the oil harvesting site for measuring the water content in the oil (Temperature 3 in Figure 17), the temperature of the other equations is associated with the temperature of the paper. The water content of the paper at the bottom (WCP 2) or top (WCP 1) can be estimated. The temperatures to be used are the lower part (Temperature 2) and the upper part (Temperature 1). The water content in the paper will be higher in the lower part of the transformer since the temperature is lower there, so there is less water transfer into the oil. However, there is a greater risk of forming bubbles in the upper part because the temperature is higher.

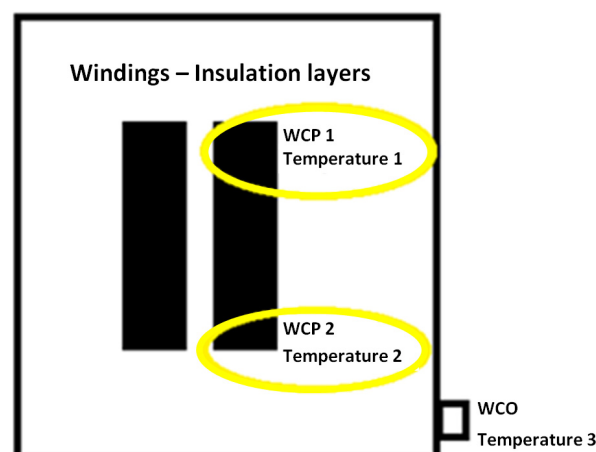


Figure 17. Temperatures for calculating water content in solid insulation.

#### 4.2.4. Limits and Definitions

The IEEE C57.106-2002 standard suggests maximum percentages of water in the solid insulation system [24] depending on the transformer voltage rating:

- <69 kV, 3% maximum
- 69 kV–230 kV, 2% maximum
- >230 kV, 1.25% maximum

Other existing standards only assign ratings for water content. For example, in [53], the IEEE 62—1995 standard recommends the following attribution of water percentages:

- Dry insulation, 0–2%
- Wet insulation, 2–4%
- Very wet insulation, >4.5%

#### 4.2.5. Temperature for Water Bubbles Occurring

An important measure to monitor the water content of the paper is the temperature at which water bubbles can occur. In [51], two relations that allow calculating the temperature of origin of water bubbles are referred to. The first (20) is an empirical formula suggested by c and Lindgren [51], depending on the WCP, the total pressure acting on the bubbles ( $Pr$ ), and the total gas content in the oil ( $g$ ).

$$T = \left[ \frac{6996.7}{22.454 + (1.4495 \times \ln(WCP)) - \ln(Pr)} \right] - \left[ e^{0.473 \times WCP} \times \left( \frac{g}{30} \right)^{1.585} \right] \quad (20)$$

The other Equation (21) was published by Koch and Tenbohlen [42] and uses two parameters that depend on the material ( $A$  and  $B$ ) and the WCP. Some typical values of these parameters are available in Table 13, which depend on the type of oil and the condition of the insulating kraft paper.

$$T = A \times e^{B \times CP} \quad (21)$$

**Table 13.** Parameters to be used in Equation (21).

Oil	Paper	A	B
Shell Diala D (new)	New	195.5	−0.11186
Shell Diala D (new)	Improved. thermally new	237.7	−0.13718
Shell Diala K 6 SX (used)	Improved. thermally used	178	−0.07338

#### 4.3. Transformer Aging Model

The aging model aims to estimate the state of solid insulation over time, which is extremely useful since there is no direct access to solid insulation instead of liquid insulation.

It is possible, as mentioned above, to estimate the degree of polymerization of the solid insulation after  $t$  years after its determination from Equation (2). It is also possible to determine the remaining lifetime by imposing a final polymerization degree, generally 200.

The activation energy of the reaction ( $E_a$ ) takes its expected value of 111 kJ/mol. The constant that depends on the chemical environment ( $A$ ) varies with water content, oxygen content, and acidity, the latter being less important. It is possible to update the estimate of the degree of polymerization depending on the sampling time of temperature, water content, and oxygen content. The temperature will be the hot spot, considered the worst case.

In [57], the value of the constant  $A$  was determined for low, medium, and high oxygen concentration, all for WCP of 0.5%, 1.6%, and 2.7%, and two types of paper, kraft, and thermally improved kraft, the determined values are shown in Table 14. From here, it is possible to determine the equations that enable the calculation of the constant  $A$  for

thermally improved kraft paper by polynomial interpolation [49], as it was done for Equations (22)–(24). The equations obtained are (25)–(27).

**Table 14.** Constant  $A$  depends on water content, oxygen concentration, and paper type (data in [14]).

Paper Type	Oxygen Concentration in Oil	Water Content on Paper	$A$
Kraft paper	Low	0.5%	1.42 (10 <sup>8</sup> )
		1.6%	6.80 (10 <sup>8</sup> )
		2.7%	1.65 (10 <sup>9</sup> )
	Average	0.5%	4.66 (10 <sup>8</sup> )
		1.6%	1.66 (10 <sup>9</sup> )
		2.7%	3.33 (10 <sup>9</sup> )
	High	0.5%	9.33 (10 <sup>8</sup> )
		1.6%	3.05 (10 <sup>9</sup> )
		2.7%	4.70 (10 <sup>9</sup> )
Thermally improved kraft paper	Low	0.5%	6.92 (10 <sup>7</sup> )
		1.6%	2.61 (10 <sup>8</sup> )
		2.7%	1.03 (10 <sup>9</sup> )
	Average	0.5%	2.70 (10 <sup>8</sup> )
		1.6%	7.32 (10 <sup>8</sup> )
		2.7%	2.03 (10 <sup>9</sup> )
	High	0.5%	4.29 (10 <sup>8</sup> )
		1.6%	2.03 (10 <sup>9</sup> )
		2.7%	4.27 (10 <sup>9</sup> )

#### 4.3.1. Kraft Paper

- Low oxygen content in oil ( $O_2 < 6000$  ppm):

$$A = 1.78 \times 10^{12} \left( \frac{WCP}{100} \right)^2 - 1.10 \times 10^{10} \left( \frac{WCP}{100} \right) + 5.28 \times 10^7 \quad (22)$$

- Average oxygen content in the oil ( $7000 \text{ ppm} < O_2 < 14,000$  ppm):

$$A = 1.30 \times 10^{11} \left( \frac{WCP}{100} \right) - 1.84 \times 10^8 \quad (23)$$

- High oxygen content in oil ( $16,500 \text{ ppm} < O_2 < 25,000$  ppm):

$$A = 1.71 \times 10^{11} \left( \frac{WCP}{100} \right) + 1.55 \times 10^8 \quad (24)$$

#### 4.3.2. Thermally Improved Kraft Paper

- Low oxygen content in oil ( $O_2 < 6000$  ppm):

$$A = 2.26281 \times 10^{12} \left( \frac{WCP}{100} \right)^2 - 2.9119 \times 10^{10} \left( \frac{WCP}{100} \right) + 1.56625 \times 10^8 \quad (25)$$

- Average oxygen content in the oil ( $7000 \text{ ppm} < O_2 < 14,000$  ppm):

$$A = 3.13223 \times 10^{12} \left( \frac{WCP}{100} \right)^2 - 1.7686 \times 10^{10} \left( \frac{WCP}{100} \right) + 2.13124 \times 10^8 \quad (26)$$

- High oxygen content in oil ( $16,500 \text{ ppm} < O_2 < 25,000 \text{ ppm}$ ):

$$A = 2.6405 \times 10^{12} \left( \frac{WCP}{100} \right)^2 + 9.0095 \times 10^{10} \left( \frac{WCP}{100} \right) - 8.74876 \times 10^8 \quad (27)$$

#### 4.4. Load Factor Monitoring Model

The load factor model is quite simple, and its purpose is to monitor the transformer load factor, which, as suggested in [50], should be lower than 200%. The load factor calculation is performed by dividing the rms value of the current by its nominal value. Whenever the load exceeds 200%, an “alarm should sound,” and one should look at the status of the transformer components and understand their operating condition. Note that the thermal model’s load factor is used as an input variable.

#### 4.5. Analysis Model of Gases Dissolved in Oil

This model involves applying the methods of analysis of gases dissolved in oil already described in Section 3.2. As previously mentioned, these are only valid when the concentration of one of the gases or the rate of change of one of the gases exceeds certain values. Table 15 summarizes the limits according to some of the most relevant standards or entities currently on the market. For “IEC Std 60599-97,” the normal values are presented, while the maximum suggested limit is presented for the others.

**Table 15.** Limits for the concentration of gases dissolved in oil. Adapted from [59], licensed under CC BY 4.0.

Standard	Gas Concentration [ppm]							
	H <sub>2</sub>	CO	CO <sub>2</sub>	CH <sub>4</sub>	C <sub>2</sub> H <sub>6</sub>	C <sub>2</sub> H <sub>4</sub>	C <sub>2</sub> H <sub>2</sub>	TCG
IEC Std 60599-97	60–150	540–900	5100–13,000	40–110	50–90	60–280	3–50	-
IEEE Std C57.104-91	100	350	2500	120	65	50	1	720
Laborelec	200	-	-	Σ C <sub>n</sub> H <sub>y</sub> < 300	-	-	-	-
CIGRE 15.01	100	Σ CO + CO <sub>2</sub> < 10,000	-	-	-	-	20	-
					Σ C <sub>n</sub> H <sub>y</sub> < 500			-

According to the IEC 60599–1999 standard, the slew rate limits are highly dependent on the type of transformer, the age, identified faults, load patterns, and the oil volume. It is suggested that a 10% gas increase per month is generally indicative of an active fault and that if there is no variation or the variation is very small (<10% in a month), the fault has possibly disappeared. A study case applied the analysis methods of the gases dissolved in the transformer oil above their normal concentration. It noticed a variation above 10% when comparing the day under analysis with the day 30 days before.

#### 4.6. Model for Monitoring and Diagnosing Crossings

The diagnosis of the condition of the capacitive type crossings can be made through several tests. The most common practices in monitoring applications are measuring the dielectric loss factor ( $\tan(\delta)$ ), the capacity (C), and the partial discharge test. For OIP type crossings, it is possible to analyze the gases dissolved in the oil and their quality, such as the oil in the transformer tank, stressing the tolerable limits. The interpretation methods vary a little.

It is possible to detect material damage, such as cracks or breaks, or even short-circuited layers, the capacity increase or partial discharges can identify that. However, to detect by-products resulting from the aging of the crossing, such as water, it is advisable to monitor the dielectric loss factor [60]. It should be noted that for RBP-type bushings, an increase in capacity can mean an oil impregnation. Two experimental tests were conducted to model the crossing monitoring: the measurement of the capacity  $C$  and the dielectric loss factor  $\text{tag}(\delta)$  to detect abnormal operating conditions due to its simplicity and common use in the industry.

For continuous measurement of the values of  $C$  and  $\text{tag}(\delta)$ , a sensor is placed in the capacitive socket that allows the connection of test equipment, as shown in Figure 18.



Figure 18. Crossing monitoring sensor [65].

IEEE C57.19.01-2000 suggests threshold values for the power factor (compared to the nameplate value) and good power factor and capacity value changes before and after the dielectric breakdown voltage test. Table 16 lists these values.

Table 16. Limits for power factor and capacity change in different types of crossing.

Type of Bushings	Power Factor ( $\cos \theta$ ) Corrected to 20 °C		Capacity
	Limit [%]	Acceptable Change	Acceptable Change [%]
OIP	0.5	+0.02/−0.04	±1.0
RIP	0.85	±0.04	±1.0
RBP	2.0	±0.08	±1.0

The weather where the transformer is installed should be considered when interpreting the values obtained for the power factor because it can be influenced by rain [9]. It can be seen in Figure 19 the evolution of the change in  $\Delta\text{tag}(\delta)$  (blue) and the rainfall measured in three meteorological stations located next to the transformer (orange, red, and purple). Furthermore, the power factor varies with temperature, converting to a common temperature base, usually 20 °C.

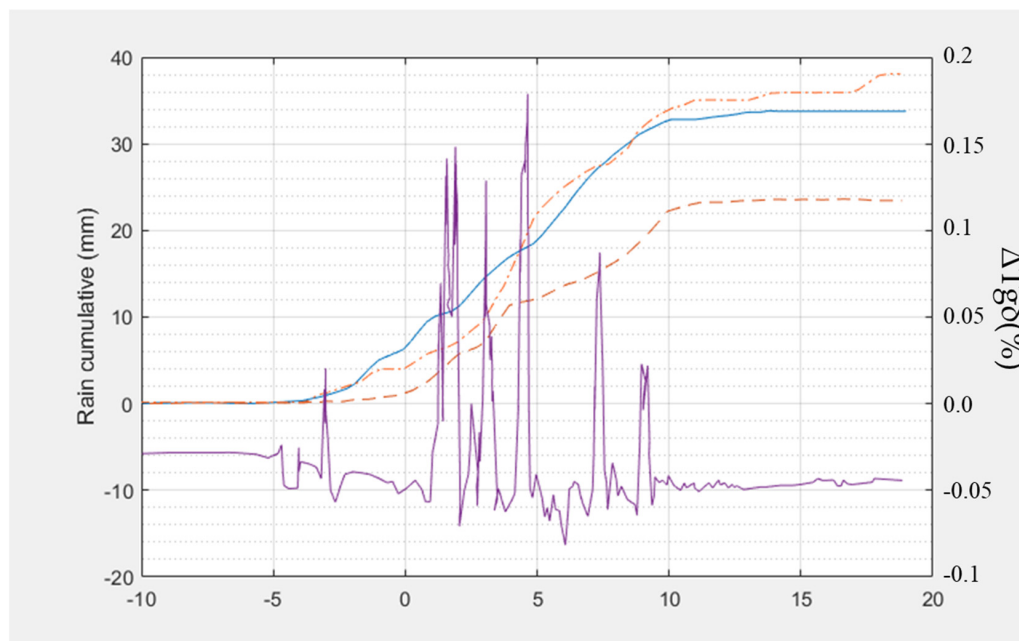


**Figure 19.** Evolution of the change in the dielectric loss factor ( $\Delta\text{tag}(\delta)$ ) depending on the amount of rain measured in 3 weather stations near a power transformer (data available in [66]). Rain cumulative at weather station 1 (blue line), rain cumulative at weather station 2 (orange dotted line), and rain cumulative at weather station 3 (red dashed line).

4.7. Model for On-Load Voltage Regulator Monitoring and Diagnosis

Of the existing methods to determine the operating condition of the voltage regulator on load, the most common in the industry that has applicability for continuous monitoring in time and automatically are: vibration measurement, motor current measurement, temperature measurement of your oil, analysis of the gases dissolved in your oil and also in the registration of its positions.

The analysis of the gases dissolved in the oil and their quality is similar to the transformer tank. For the on-load voltage regulator, as for the crossings, the interpretation methods and the tolerable limits are different.

Temperature is an important indicator of the operating condition of the on-load voltage regulator, as temperatures close to or above the tank generally indicate internal problems. However, the temperature is normal for some voltage regulators operating above the tank [62].

Table 17 summarizes the method’s sensitivity for detecting voltage regulator failures. Green color corresponds to excellent/very good sensitivity, yellow to good/fair and red to poor sensitivity. For all measurements/tests, except for mechanical vibrations, the sensitivity is the same for all types of regulators. For mechanical vibrations depending on whether the transformer uses resistance or reactance in switching or a vacuum type, the sensitivity changes according to the type of abnormal operating condition to be detected.

**Table 17.** Sensitivity of tests for detecting anomalies. Adapted from [22] and [67].

Abnormal Operating Conditions	Measurements/Testes					
	Temperature	Analysis of Gases Dissolved in Oil	Motor Electric Current	Vibrations		
				Resistance	Reactance	Vacuum
Contact wear				X	X	X
Overheating	X	X		X	X	X
Transition timing				X	X	X

Table 17. Cont.

Abnormal Operating Conditions	Measurements/Testes					
	Temperature	Analysis of Gases Dissolved in Oil	Motor Electric Current	Vibrations		
				Resistance	Reactance	Vacuum
Alignment contacts			X	X	X	X
Electric arc		X		X	X	X
Sequence/Timing				X	X	X
Motor			X			
Brake			X			
Lubrication			X			
Control/Relays			X			
Connections/Gears			X	X	X	X

By analyzing Table 17, it is concluded that it is possible to determine the operating condition of the on-load voltage regulator by monitoring vibrations, oil temperature, and engine current. Along with these three measurements, it is vital to know the contact's position. Its position will also be one of the measurements for this model.

#### 4.8. Cooling System Monitoring Model

The cooling system is monitored by comparing the measured hot spot and top oil temperatures with temperatures estimated by the thermal model. Knowing which type of cooling the transformer is at any given moment, it is possible to estimate the hot spot temperatures and the top of the oil by the thermal model and compare them with the measured temperatures. If temperatures are very different, it probably means that the cooling system is not working normally.

### 5. Case study in a 1400 MVA Three-Phase Large-Power Transformer

A phase-shifting 1400 MVA three-phase transformer was available to study with record data of its service since 2007. Phase-shifting transformers are composed of two units: the main is called the *excitation unit*; the other is designated as the *serial unit*. For large-power transformers, each unit is placed in a different tank. This is the case of this transformer, which has nominal voltage on the primary and secondary sides of 400 kV and allows variation of the phase shift between  $\pm 25^\circ$ . The transformer oil used is the Nynas Nytro 10XN oil, a standard transformer oil. As for the transformer cooling system is known that it is ONAF (Oil Natural Air Forced). However, no further information on whether or not the type of cooling varies with temperature and/or power was available.

The transformer under analysis began to show signs of abnormal operating conditions in 2012, indicated by the analysis of gases dissolved in the transformer oil. Consequently, the transformer began to be monitored more frequently, carrying out tests. However, it was impossible to determine the cause of the gas increase. Therefore, in 2014, an online multi-gas DGA monitor was installed to automatically measure some gas and water concentration in the oil, permanently installed in the transformer. The gases measured were hydrogen ( $H_2$ ), acetylene ( $C_2H_2$ ), ethylene ( $C_2H_4$ ), and carbon monoxide (CO). The DGA monitor (Hydrocal 1005) analyses the evolution of gases daily without requiring a team to travel to the site to collect oil, aiming to understand the cause of the anomalies from the data collected.

#### 5.1. Measured Quantities

The data collected was of two types: data obtained continuously and automatically (*online*), and data obtained by measurements made on-site by technicians, sporadically

(*offline*). Note that *offline* data were only used as a reference to verify the validity of *online* data.

#### 5.1.1. Online Quantities and Their Variables' Representation

- Primary and secondary voltage (U1 and U2);
- Apparent, reactive, and active power (MVA, MVAR, and MW);
- Position of the on-load voltage regulator (TAP);
- *Excitation* (EX) and *series* (SE) *unit* temperatures (Temp\_Windings\_EX and Temp\_Windings\_SE), and;
- Concentration of gases (C<sub>2</sub>H<sub>2</sub>, C<sub>2</sub>H<sub>4</sub>, H<sub>2</sub>, and CO) and water in oil, in ppm, measured in the *excitation unit*.

#### 5.1.2. Offline Quantities and Their Variables' Representation

- Gas concentration: H<sub>2</sub>, O<sub>2</sub>, N<sub>2</sub>, CO, CO<sub>2</sub>, CH<sub>4</sub>, C<sub>2</sub>H<sub>4</sub>, C<sub>2</sub>H<sub>6</sub>, and C<sub>2</sub>H<sub>2</sub>;
- Concentration of water in oil;
- Furans: 5-hydroxymethyl-2-furfural (5HMF), 2-furfuryl alcohol (2FOL), 2-furfural (2FAL), 2-acetyl furan (2ACF), 5-methyl-2-furfural (5MEF);
- Oil Quality (Color, Appearance, Density, Neutralizing Number, Dissipation Factor (90 °C), Disruption Voltage, Phenolic Inhibitor, Presence of Insolubles, Precipitated Substances), and;
- Oil temperature at the bottom.

### 5.2. Data Quality

#### 5.2.1. Remote Sensing

From the *online* data available, except for the concentration of gases and water in the oil, there was no information on how they were obtained nor the location of the device/sensor that measured or estimated them. However, one assumed that the voltage values U1 and U2 refer to phase-to-phase rms values and the powers reflect these rms values.

The device measuring the concentration of gases and water, the Hydrocal 1005, was placed in one of the valves at the bottom of the transformer in the *excitation unit*. The relative precision of each gas measurement is indicated in Table 18, taken from the Hydrocal equipment manual. The measurement of CO, C<sub>2</sub>H<sub>2</sub>, and C<sub>2</sub>H<sub>4</sub> is done through infrared spectroscopy; the measurement of H<sub>2</sub> is achieved using a proprietary microelectronic sensor, and the measurement of H<sub>2</sub>O is done with a capacitive sensor.

**Table 18.** Gas measurement precision from Hydrocal.

H <sub>2</sub>	±25 ppm
C <sub>2</sub> H <sub>2</sub>	±5 ppm
C <sub>2</sub> H <sub>4</sub>	±10 ppm
CO	±25 ppm
H <sub>2</sub> O	±3 ppm

*Offline* data is measured by a laboratory specialized in oil collection and analysis. It is known that the oil collection is done in the same valve where the Hydrocal is located. The result for each parameter follows a standard/technique, with Table 19 showing a systematization of the standards used for each parameter.

**Table 19.** Quantities and technical standards are used by a specialized laboratory.

Quantity	Norma
Gases	IEC 60567
Water	IEC 60814

Table 19. Cont.

Quantity	Norma
Furans	IEC 61198
Color and appearance	ISO 2049
Density (20 °C)	ASTM D4052
Neutralizing number	IEC 62021-1
Breakdown voltage	IEC 60156
Dissipation factor	IEC 60247
Phenolic inhibitor	IEC 60666
Sludge and sediment	IEC 60422

5.2.2. Sampling

Online data was obtained and listed in a “sheet” where each variable was sampled at each 2 min, as shown in Figure 20. Data contains information about the primary U1 and secondary voltage U2 (“U rails 1” and “U rails 2”), apparent power (“MVA”), reactive power (“MVAR”), active power (“MW”), the on-load voltage regulator (“TAP”), excitation and series unit temperatures (“Temp Wick EX” and “Temp Wick SE”), the concentration of gases (“C<sub>2</sub>H<sub>2</sub>”, “C<sub>2</sub>H<sub>4</sub>”, “CO”, and “H<sub>2</sub>”), and water in oil (“Moisture”).

	U rails 1	U rails 2	MVA	MVAR	MW	TAP	Temp Wick EX	Temp Wick SE	C2H2	C2H4	CO	H2	Moisture
	WSDAPP738ACC_PODIEquip ment1PDKF15026188IU(NV)												
00:00:00	408.1598816	408.079956	-298.94901	8.12249947	-298.83749	13	37,3143	33,2178	1.86558473	13.8495522	31.7090359	55.46106	7.114054
00:02:00	408.2670898	408.205688	-276.914	5.92439985	-276.85498	13	37,263	33,064	1.86493897	13.8735714	31.7090359	55.44814	7.113703
00:04:00	408.4072876	408.387085	-291.14349	4.61319971	-291.12402	13	37,263	33,064	1.86429322	13.8975906	31.7090359	55.43522	7.113352
00:06:00	408.5474854	408.568481	-296.909	3.30200005	-296.909	13	37,263	33,064	1.86364746	13.9216099	31.7090359	55.4223	7.113001
00:08:00	408.6877136	408.749908	-298.06601	1.99080002	-298.06601	13	37,263	33,064	1.86300017	13.9456301	31.7090359	55.40937	7.11265
00:10:00	408.8279114	408.931305	-293.05249	0.6796	-293.05249	13	37,263	33,064	1.86235595	13.9696493	31.7090359	55.39645	7.112299
00:12:00	408.568512	408.671509	-287.2865	2.2414999	-287.26801	13	37,263	33,064	1.86171019	13.9936686	31.7090359	55.38353	7.111948
00:14:00	408.3471375	408.460144	-270.01199	6.67649984	-269.91351	13	37,263	33,064	1.86106443	14.0176878	31.7090359	55.37061	7.111597
00:16:00	408.563385	408.738373	-233.356	4.45900011	-233.276	13	37,263	33,064	1.86041868	14.041707	31.0145912	55.35769	7.111247
00:18:00	408.7796326	409.016632	-216.11426	0.024	-216.11426	13	37,263	33,064	1.85977292	14.0657263	31.0145912	55.34477	7.110896
00:20:00	408.9958801	409.294861	-208.78674	0.024	-208.78674	13	37,263	33,064	1.85912716	14.0897465	31.0145912	55.33185	7.110545
00:22:00	409.2586365	409.537109	-197.7955	0.024	-197.7955	13	37,263	33,0127	1.85848141	14.1137657	31.0145912	55.31893	7.110194
00:24:00	409.5678711	409.743378	-193.59775	2.14499998	-193.55325	13	37,263	32,9101	1.85783565	14.137785	31.0145912	55.30601	7.109843
00:26:00	409.8771362	409.949615	-199.85725	6.38700008	-199.72375	13	37,263	32,8075	1.85718989	14.1618042	31.0145912	55.29309	7.109492
00:28:00	410.1863708	410.155884	-197.537	7.90200043	-197.4095	13	37,263	32,7049	1.85654414	14.1858234	31.0145912	55.28017	7.109141
00:30:00	410.3684998	410.30368	-199.37601	6.69000006	-199.33749	13	37,263	32,6023	1.85589838	14.2098436	31.0145912	55.26725	7.10879
00:32:00	410.4234924	410.393005	-187.38251	5.47800016	-187.38251	13	37,263	32,4997	1.85525262	14.2338629	31.0145912	55.25433	7.108439

Figure 20. Online data is listed in a “sheet” sampled every 2 min.

The sampling of voltages is variable. When one is measured, the other is not always measured. In general, they were measured every twenty minutes. It was verified that voltage variation was minimal for adjacent samples. Hence, the error is very small using a linear interpolation every two minutes.

Active power is measured practically every two minutes, and it varies greatly. Reactive power is more irregularly sampled but is measured several times an hour, on average ten times, and there is much less variation than active power. It is concluded that interpolating the powers every two minutes, the error will be small. For apparent power, the sampling should be similar. As such, values interpolated every two minutes for this one were also considered valid.

The TAP variable is only measured when there is a change in the voltage regulator position. It has been found that there can be several position switches in a minute and that a long time can also pass without switches. Thus, the interpolation of this variable from

two minutes to two minutes was made, keeping the measured position until there was a new measurement.

The temperature had a very small variation between samples and is almost always measured every twenty minutes. Therefore, linear interpolation for every two minutes did not make a significant error.

The concentration of gases obtained by Hydrocal has a different sampling time for each of them. However, the amount of sampling for each one per day is similar. Carbon monoxide is measured on average thirty/forty times a day. For this, linear interpolation every two minutes is considered reasonable since its variation between adjacent samples is small. However, sampling is carried out on average four times a day for the remaining gases. Therefore, interpolating the data every two minutes will make a significant error. So, it was chosen to place all gases daily, making daily averages of the measurements made. One proceeded the same way for water since this sampling was carried out four or five times daily.

It was verified that some values deviated greatly from the others for the gases. Since the gases' evolution was practically constant, without great fluctuations, these values considered spurious were eliminated.

Offline data: sampling time of offline data varies greatly and is done depending on the results of previous tests. For example, when gases showed a very large increase from a previous report, a new analysis of the gases was performed after a few days. If all is well, follow the normal sampling period, which varies from company to company, usually one to two years.

### 5.3. Load Factor

The load factor results from dividing the current by the rated current. In the absence of measured current (I) values, this was obtained from the existing relationship (Equation (28)) with voltage (U) and apparent power (S).

$$I = \frac{S}{\sqrt{3}U} \quad (28)$$

The evolution of the primary voltage U1 and apparent power S1 ("MVA") are presented in Figures 21 and 22, respectively. The voltage has an approximately constant value over time. The apparent power varies greatly and alternates between negative and positive values, corresponding to the power transit taking place to one side.

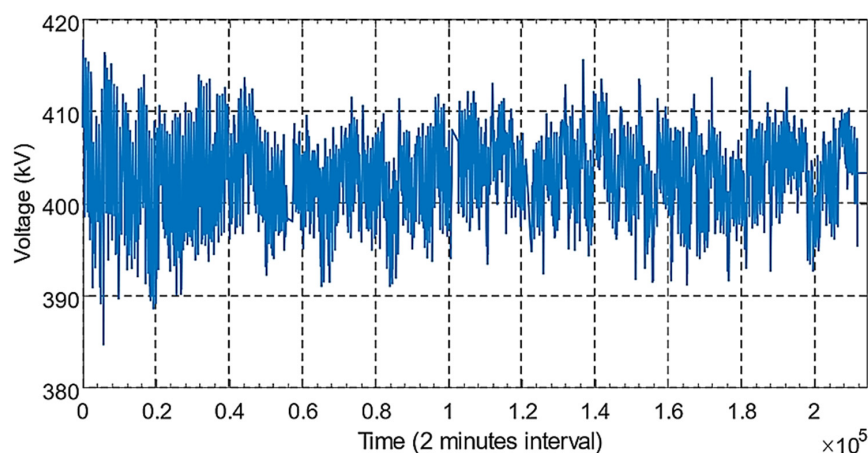


**Figure 21.** Evolution of the primary voltage U1.

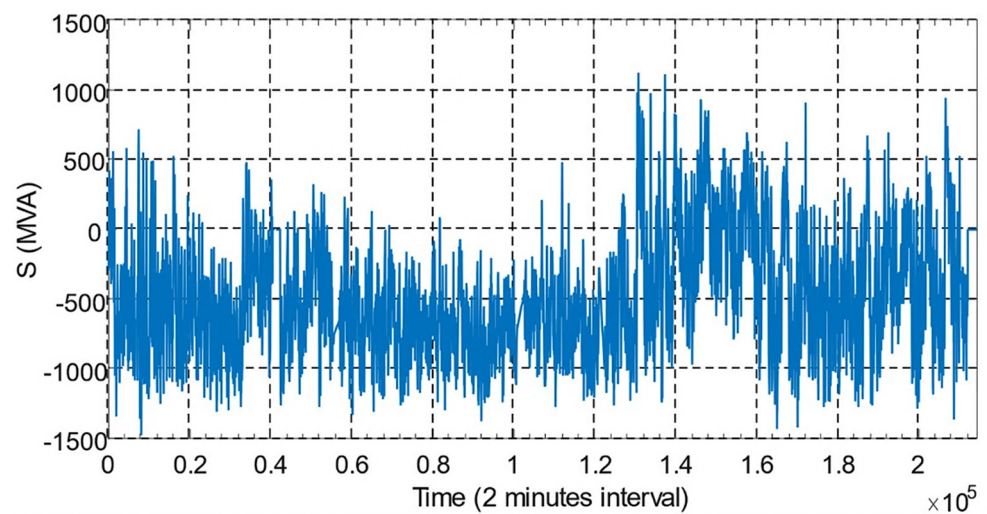


Figure 22. Evolution of apparent power  $S_1$  (“MVA”).

Figure 23 shows the load factor for weekdays (2nd to 6th) related to the first week of February. Figure 24 shows the load factor for the weekend. There is a similar pattern for weekdays, which significantly differs from the pattern on weekend days.

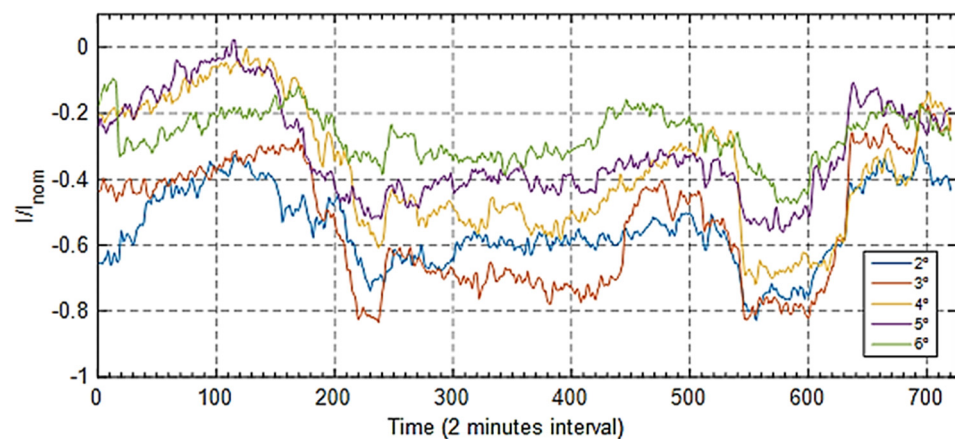


Figure 23. Evolution of the load factor for different working days (2nd to 6th) of the first week of February.

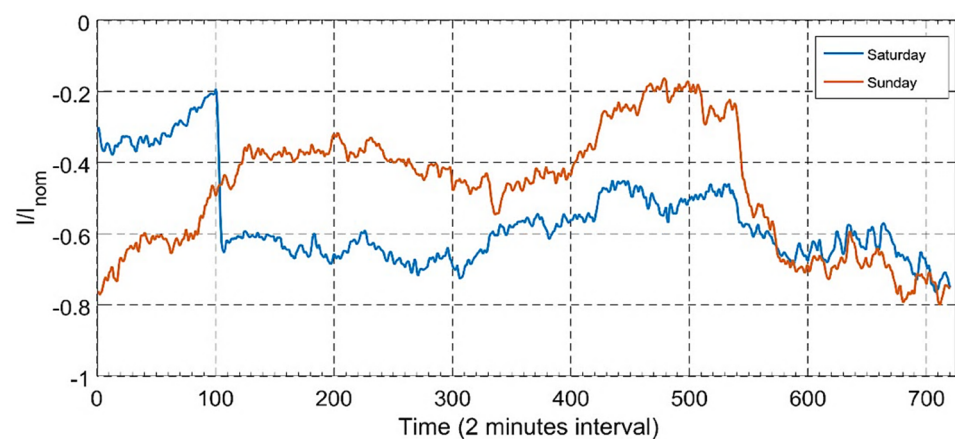
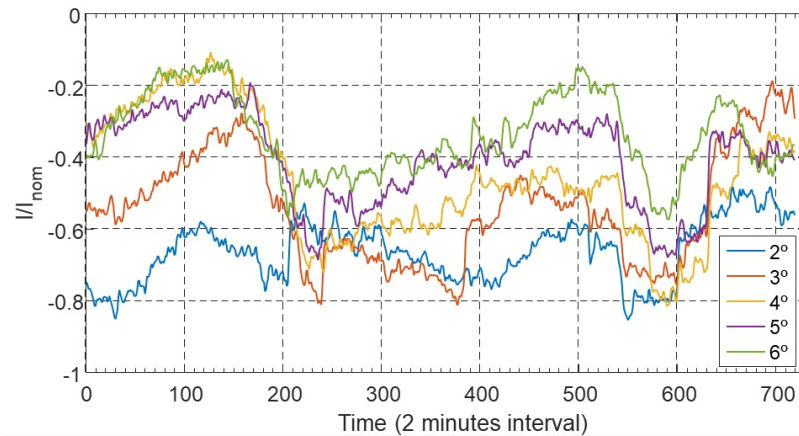


Figure 24. Evolution of the load factor for weekend days of the first week of February.

After checking the load factor for several months and weeks, it was concluded that load patterns depend on whether a weekday or a weekend day. One also verified the existence of seasonality in the patterns. For example, Figure 25 shows the load factor during the second week of February. It shows the same seasonal pattern taken the week before (Figure 23) for the same month.



**Figure 25.** Second week of February: evolution of load factor for different working days (2nd to 6th), presenting a similar pattern as the first week.

Figures 26 and 27 show the summer season's first and second weeks of July. The pattern, in this case, is different from the pattern of February. Both figures indicate the July pattern.

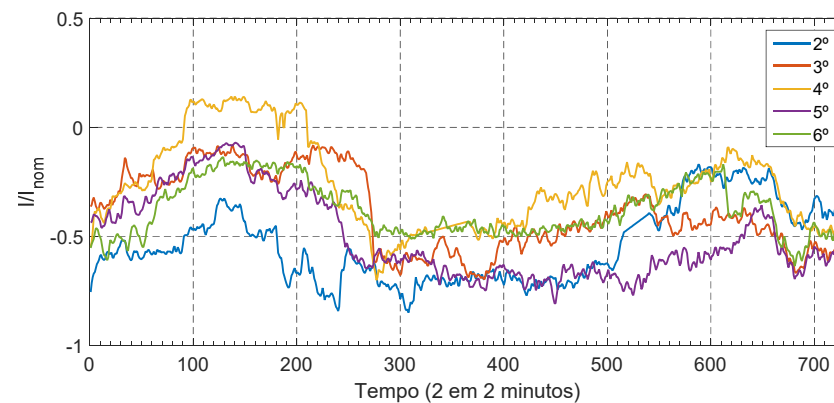


**Figure 26.** First week of July: evolution of load factor for different working days (2nd to 6th).

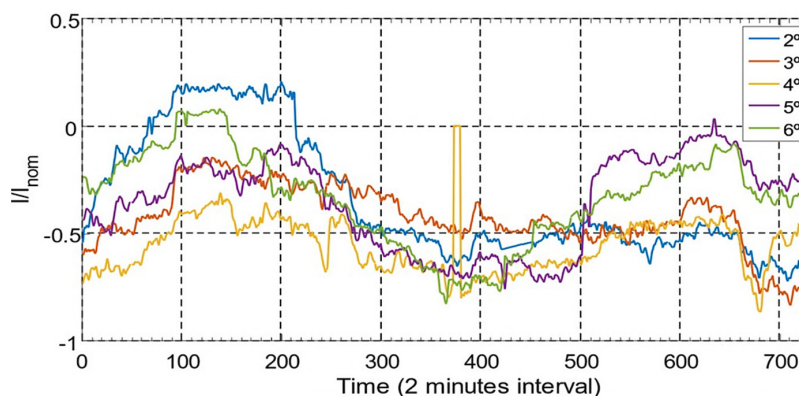


**Figure 27.** Second week of July: evolution of load factor for different working days (2nd to 6th), presenting a similar pattern as the first week.

#### 5.4. Temperature

Although there was no information on whether the temperature related to the online data was measured or estimated and which part of the transformer it represents, the temperature was assumed to refer to the windings. Observing Figure 28, which shows the evolution of the load factor in blue and temperature in orange, it can be seen that, except at the beginning, temperatures are in line, albeit with a small delay, with the load variations, i.e., it is certainly representative of the temperature of a location in the transformer.

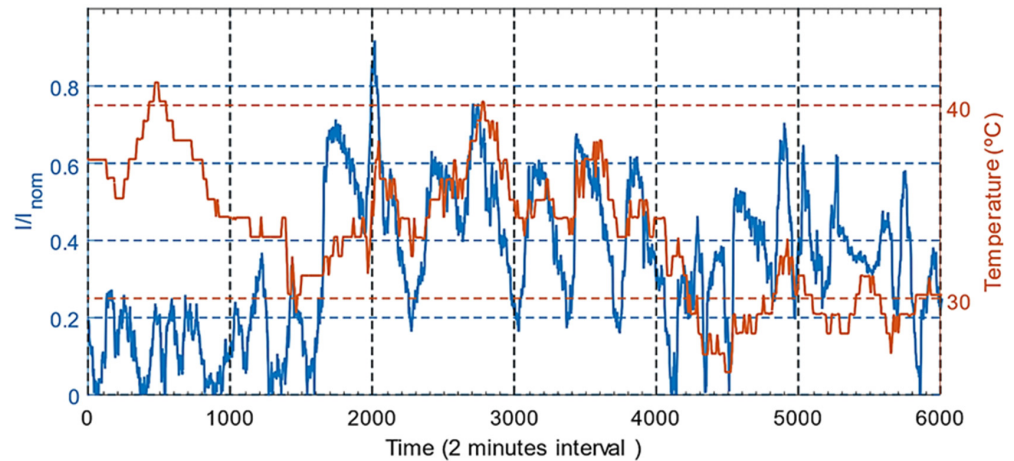


**Figure 28.** Evolution of load factor (blue) and temperature (orange). Despite a small delay, temperatures align with the load variations, becoming representative of the temperature of a location in the transformer.

Figure 29 shows the evolution of the “supposed” temperature of the windings interpolated every two minutes, in blue, and the *offline* temperature, in orange. As it is only measured when taking oil samples from the transformer, the *offline* temperature is only known on the collection day, with no information on the time of day it was measured. Thus, the measured temperature value is assigned to the entire measurement day to compare *online* and *offline* temperatures. It can be seen in Figure 28 that the *online* temperature (blue) is almost always lower than the *offline* temperature, which is not possible since the *online* temperature supposedly refers to the temperature of the windings and the *offline* temperature represents the temperature at the bottom of the oil, which is always lower than the temperature of the windings. Thus, the location that the online temperature might represent remains unknown.

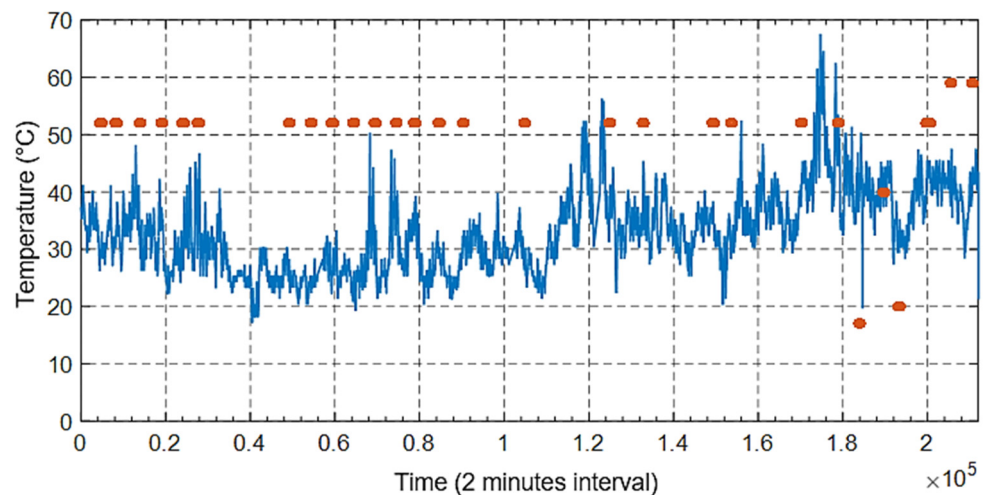


**Figure 29.** Online (blue) and offline (orange) temperature evolution.

### 5.5. Position of the On-Load Voltage Regulator (TAP)

Recording the position of the on-load voltage regulator is very important to determine its status. In this way, it is possible to understand which socket will likely have the most wear. It allows calculating switching averages or associating them with other records, such as mechanical vibrations, to understand which sockets are having problems.

Figure 30 shows the number of times each socket switched. Socket zero has the highest number of switching. As such, it is considered to present greater wear, followed by socket ten, which also presents a high number of commutations. A comparative analysis between the switching dates and their frequency also found that there is no daily or seasonal pattern for the voltage regulator positions.

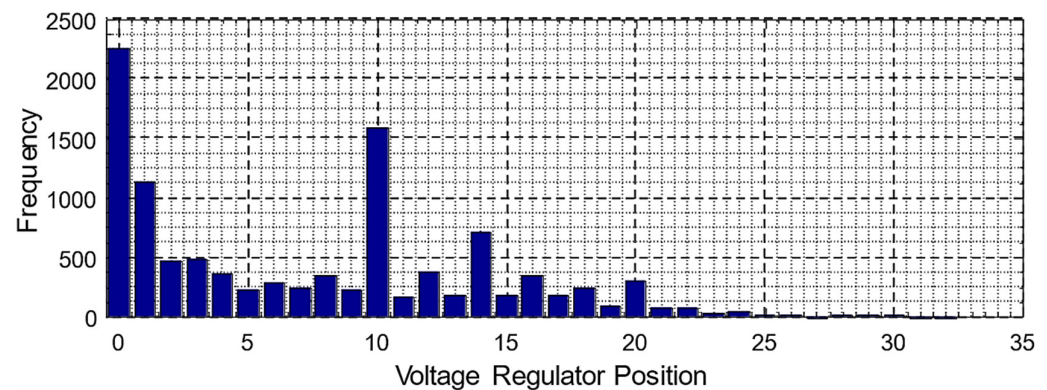


Figure 30. Frequency of socket positions taken by the on-load voltage regulator.

### 5.6. Dissolved Gases in Transformer Oil: Online and Offline

The following graphs show the evolution over time of the concentration of acetylene ( $C_2H_2$ ) in Figure 31, ( $C_2H_4$ ) ethylene in Figure 32, ( $H_2$ ) hydrogen in Figure 33, and carbon monoxide (CO) in Figure 34. The daily values of the *online* data are represented in blue, obtained by making daily averages of the data measured by Hydrocal. *Offline* data measured by the specialized laboratory is shown in orange. To compare the values of the *online* and *offline* measurements, the root-mean-square error (ERMS), the mean absolute error (AEM), and the mean relative error (RME) were calculated, which are listed in Table 20.

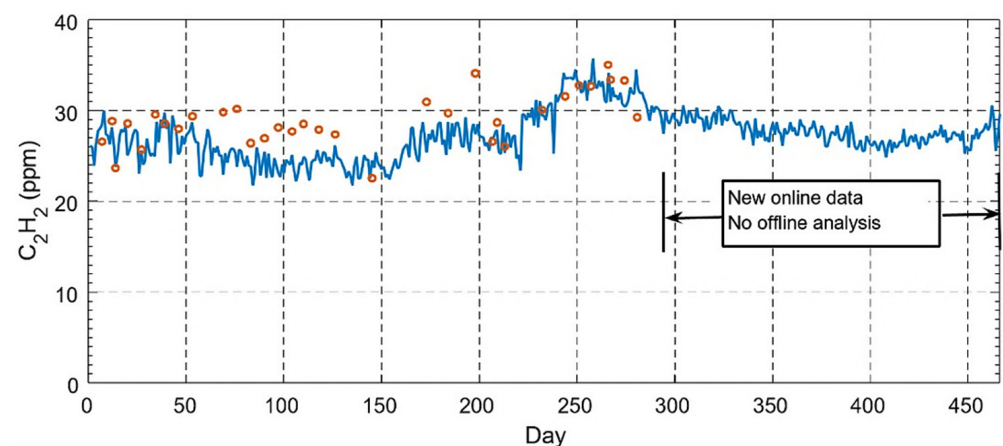
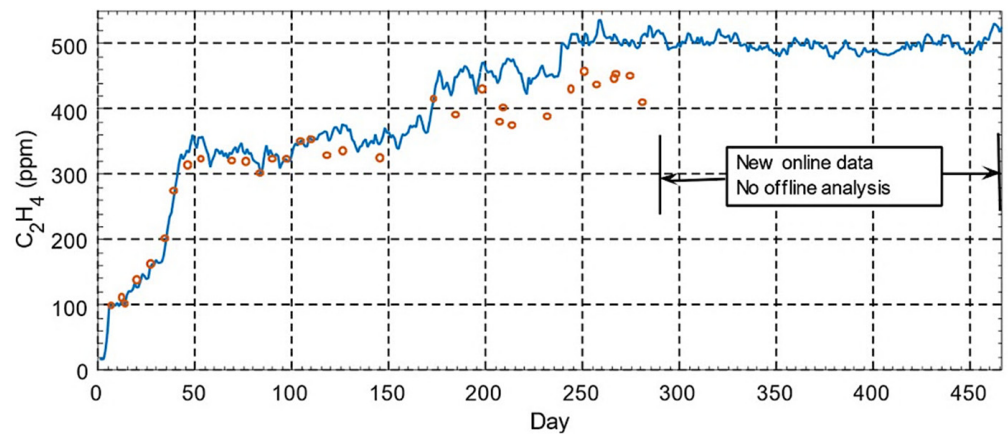
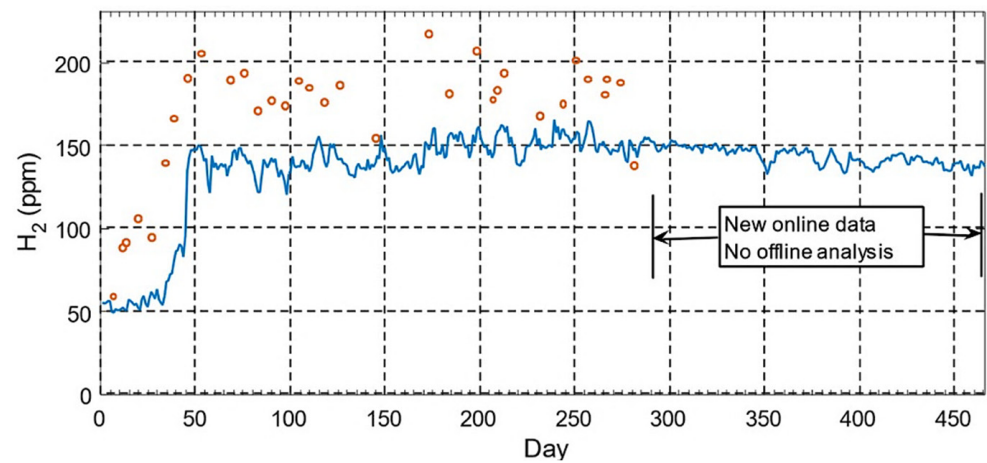


Figure 31. Evolution of acetylene concentration ( $C_2H_2$ ) over time, *online* (blue) and *offline* (orange) data.



**Figure 32.** Evolution of ethylene concentration ( $C_2H_4$ ) over time, online (blue) and offline (orange) data.



**Figure 33.** Evolution of hydrogen ( $H_2$ ) concentration over time, online (blue) and offline (orange) data.

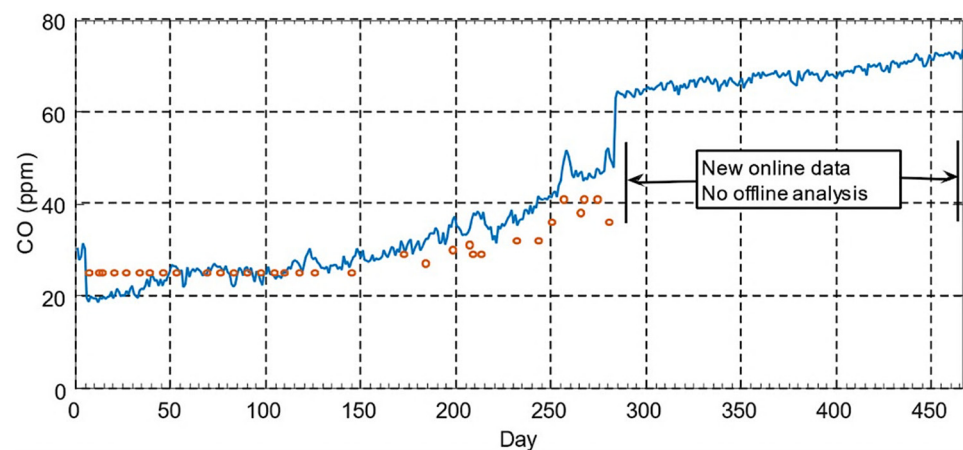


**Figure 34.** Evolution of carbon monoxide ( $CO$ ) concentration over time, online (blue) and offline (orange) data.

**Table 20.** Mismatch between online and offline measurements of gas concentration.

Gases	Error Root Mean Square (ERMS)	Absolute Mean Error (AEM)	Relative Mean Error (RME)
C <sub>2</sub> H <sub>2</sub>	3.07 ppm	2.35 ppm	8.01%
C <sub>2</sub> H <sub>4</sub>	45.93 ppm	34.77 ppm	9.6%
H <sub>2</sub>	43.93 ppm	40.22 ppm	25.0%
CO	5.48 ppm	4.45 ppm	14.91%

Observing the evolution of the acetylene concentration in Figure 31, it can be seen that, despite being too high compared to the limit of the IEEE standard (IEEE Std C57, 104–91 in Table 14), in general, it had an approximately constant behavior. It is also shown that *online* and *offline* data are very close.

Figure 32 shows the evolution of the ethylene concentration (C<sub>2</sub>H<sub>4</sub>) by taking three distinct regions. Between day 0 and day 50, there was a sharp ethylene concentration increase. In the second region, the increase is softer between 50 and day 250. The concentration stabilizes in the third region (between 250 and the end). Once again, the values of the *online* and *offline* measurements are very close, with a greater discrepancy from approximately the 180th (beginning of May) onwards.

Figure 33 presents the evolution of hydrogen concentration. Although the *online* and *offline* data tend to be quite similar, the values generally present a constant offset of 40 ppm on average. The hydrogen concentration shows a sharp increase at the beginning (between 30th and 50th, which belongs to December) and then stabilizes.

At last, Figure 34 shows the evolution of carbon monoxide concentration. It can be concluded that it had a practically constant growth rate over time, and the *online* and *offline* data were relatively close. All *offline* carbon monoxide values before day 150 are less than 25 ppm, not knowing exactly what values it takes. Thus, it was decided to assign the worst case, that is, until day 150, all *offline* samples take the value of 25 ppm.

Table 20 shows that acetylene and carbon monoxide have small deviation errors between *online* and *offline* measurements. The uncertainties in both measurements justify the deviation in these two gases. On the other hand, hydrogen and ethylene have very high absolute error values (*REQM* and *EAM*). For hydrogen, this error is caused by the general offset verified, which is probably due to a Hydrocal calibration error. The error in the ethylene table is essentially due to the discrepancy observed from May (approx. day 180). It is believed that this discrepancy may be due to the increase in summer temperature and the difference in load patterns. The errors in Table 20 were calculated using Equations (29)–(31).

$$REQM = \sqrt{\frac{\sum_{i=1}^n (x_i - y_i)^2}{n}} \quad (29)$$

$$EAM = \frac{1}{n} \sum_{i=1}^n |x_i - y_i| \quad (30)$$

$$ERM = \frac{1}{n} \sum_{i=1}^n \left| \frac{x_i - y_i}{x_i} \right| \quad (31)$$

### 5.7. Water

The water concentration in oil varies with temperature, increasing when temperature increases and vice versa. Figure 35 shows the temperature evolution available in the *online* data in blue and the evolution of water content in the oil in orange. Despite a small delay between water and temperature values, in most cases, when the temperature increases, the water content also increases, and the opposite is also true.

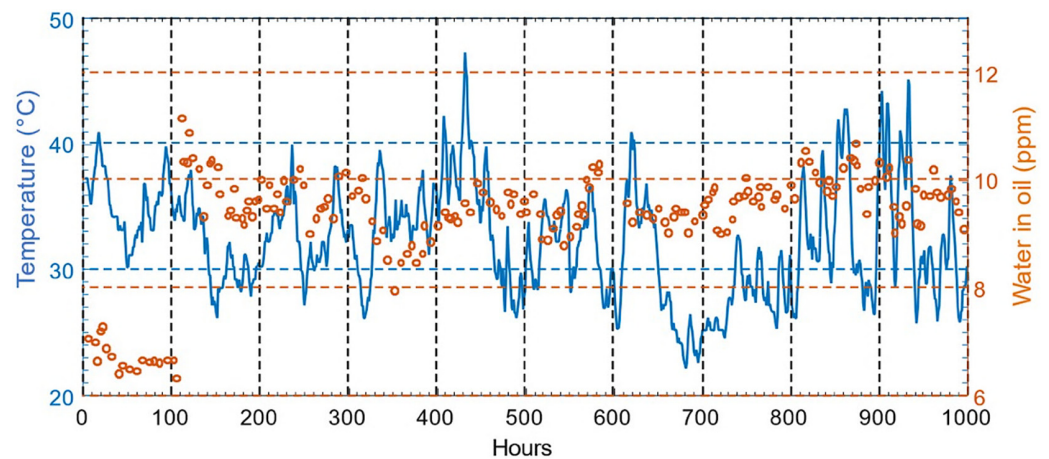


**Figure 35.** Evolution of temperature (blue) and oil (orange) water content.

To compare the measurements made by Hydrocal (*online*) and those carried out by the specialized laboratory (*offline*), it is necessary to place the water values in the same temperature reference adopted by the specialized laboratory. The formula is expressed by Equation (32) [24] to adjust water values for the same reference.

$$WCO(20\text{ }^{\circ}\text{C}) = WCO(T) \left[ 2.24e^{-0.04T} \right] \quad (32)$$

A correction was made using water measurements and the temperature available for the same hour, corresponding to an average of the temperatures for online data. For *offline* data, a correction was made using water and temperature measurements, with both measured at the bottom of the transformer.

Figure 36 shows the various measurements of water-in-oil concentration made by Hydrocal but corrected to 20 °C, in blue, and the laboratory measurements also corrected to 20 °C, in orange. For a day, there are several measurements *online* (on average 3/4), while only one is taken if there is an *offline* measurement. In this way, the *offline* measurement performed on that day was associated with the various *online* measurements.

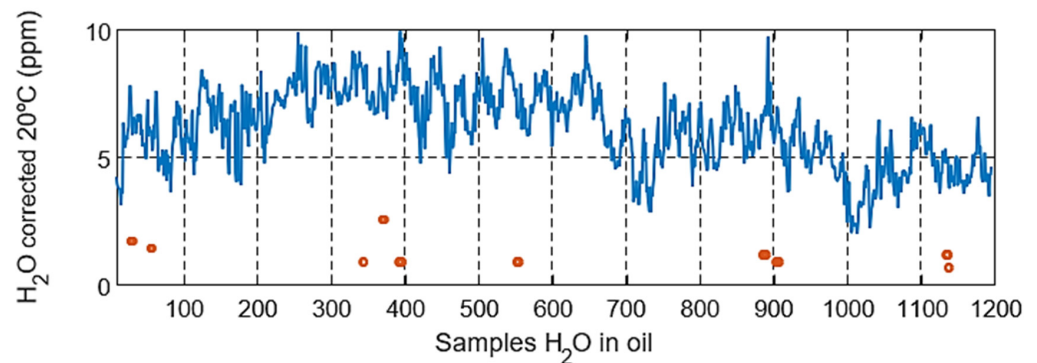


**Figure 36.** Evolution of water content in oil corrected to 20 °C, online (blue) and offline (orange) data.

Results in Figure 36 show that *offline* and *online* water concentration measurements are quite discrepant. That difference can be explained because it is uncertain where the temperature was obtained *online*. Therefore, the correction is not coherent, reinforced by the discrepancy observed for the *online* and *offline* temperatures introduced in Section 5.2. The difference between *online* and *offline* data may also be due to the measurement uncertainty, which in the case of Hydrocal is  $\pm 3$  ppm. For measurements performed by the specialized laboratory, this value is not quantified. Still, it can be high, which is evidenced by the fact that, depending on the laboratory, the result can vary greatly [68]. Figure 37 shows the results of measurements of the water-in-oil concentration of three different samples

carried out by seven laboratories (A to G) in Europe. It can be seen that the measurements are very different.

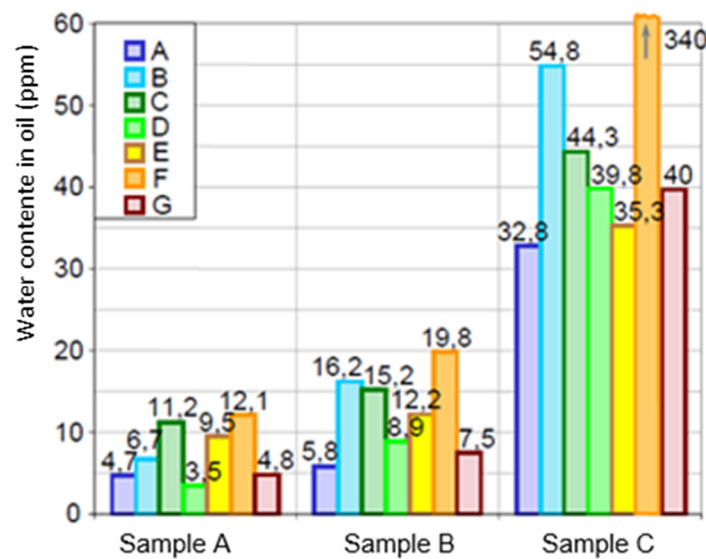


**Figure 37.** Several laboratories carried out measurements of water content in oil [68].

#### 5.8. Application of the Online Diagnostic Thermal Model

The online thermal model described in Section 4.2 for continuous monitoring analyzed the phase-shifting large-power transformer data. To apply the model, one needs the load factor and the ambient temperature on a time basis of fewer than 3.5 min because the thermal time constant associated with the windings was assumed to be 7 min.

The load factor is obtained by dividing the current by the rated current. The current is obtained by dividing the apparent power by the multiplication of the compound voltage by a root of three. Therefore, the apparent power and the compound voltage are interpolated for two-by-two minutes, which was the time base to consider.

The ambient temperature is accessed at that time base. One used [24], which allows easy access, by downloading a CSV file, to historical data from daily meteorological records, namely minimum, maximum, average temperature, wind speed and direction, humidity, dew point, precipitation, and pressure at sea level. For the intended period, between November and December of the following year (period for which load factor information is available), the only information available was obtained approximately twenty-five kilometers from the substation where the transformer was located.

As the ambient temperature is intended to be collected every 2 min, it was necessary to reproduce a typical daily temperature cycle. In [69], several models are suggested that allow simulating the daily cycle of temperature being. The “wave” model was chosen since it had the highest accuracy. According to the model, the day is divided into two segments: one from sunrise to 14:00 and from 14:00 to sunrise, while for the second segment, the minimum temperature of the following day must be used. It is assumed that the maximum temperature is at 14:00 h, the minimum temperature is at sunrise, and the remaining temperatures are calculated through Equations (33) and (34), where  $TAVE$  is the average between the minimum and maximum temperatures,  $AMP$  is defined as half the difference between the maximum and minimum temperature,  $RISE$  is the time of sunrise in hours,  $H$  is the time in hours,  $T(H)$  is the temperature at the hour  $H$  and  $H'$  is defined as  $H' = H + 10$  if  $H < RISE$  and  $H' = 14$  if  $H > 14:00$  h.

$$T(H) = TAVE + AMP \cdot \left( \cos \left( \frac{\pi \cdot H'}{10 + RISE} \right) \right) \quad (33)$$

$$T(H) = TAVE - AMP \cdot \left( \cos \left( \frac{\pi \cdot (H - RISE)}{14 - RISE} \right) \right) \quad (34)$$

Equation (33) is valid for hours between 00:00 h and sunrise and from 14:00 h up to 24:00 h. Equation (34) is valid for the interval between sunrise and 2:00 pm. However, there was an error in the expression of  $H'$  from 14:00 h since if it is constant and equal to 14, the temperature will also remain constant from 14:00 h, which does not agree with the graph obtained by the model. We then tried replicating the graph obtained in [69] to correct the expression  $H'$ . With  $H' = 14 - H$  if  $H > 14:00$  h, the graph obtained is the same as in [69], as shown in Figure 38.

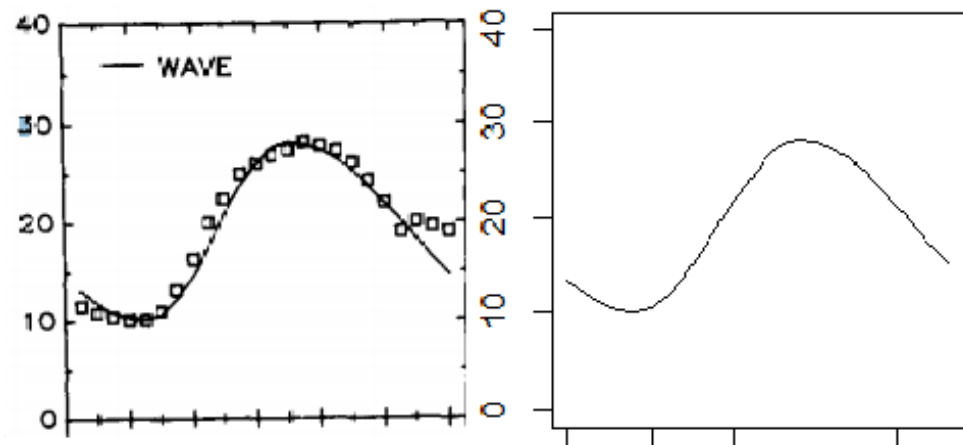


Figure 38. Left: “wave” model [69]. Right: waveform replication of the original article.

To apply the model, it is only necessary to define the time of sunrise. It was possible to obtain historical information regarding the sunrise and sunset from a weather database [70]. With all variables defined, the ambient temperature was simulated, visualizing in Figure 39 the temperature cycles simulation for the first five days of November.

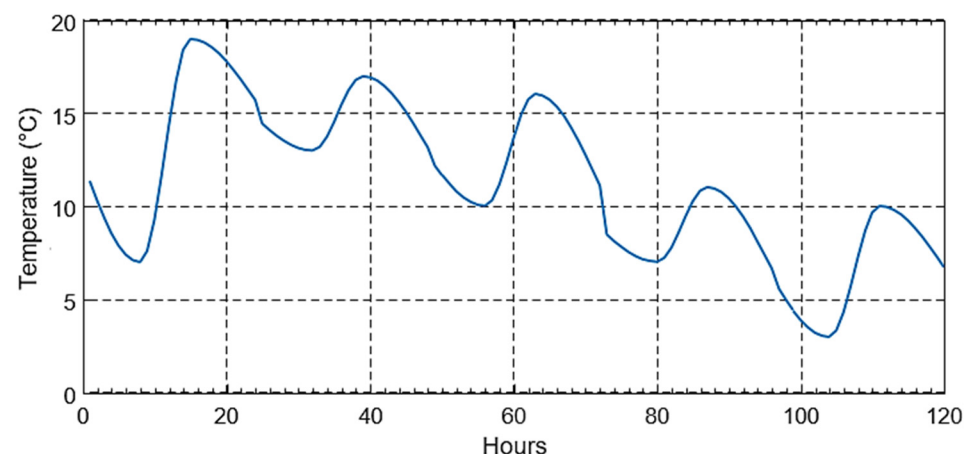


Figure 39. The Wave model simulates the daily ambient temperature cycle for the first five days of November.

To verify if the daily simulation of the ambient temperature is close to the ambient temperature in the place where the transformer is located, we obtained the hourly temperature for the place closest to the substation. The hourly temperature data measured at the substation have only existed since 2016. Thus, the data measured at 5 km and simulated from data at 25 km were compared for the first 5 days of January and the first 5 days of August. The result is shown in Figures 40 and 41, respectively. The errors shown in Table 21 were also determined.

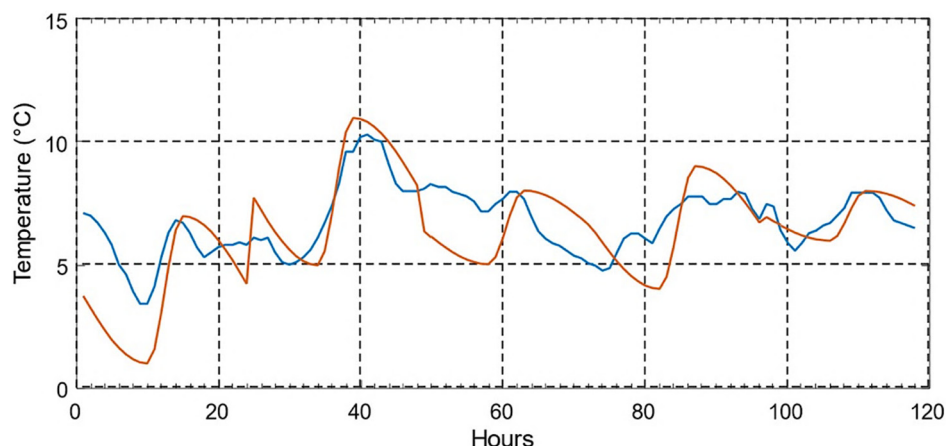


Figure 40. Simulated (blue) and measured (orange) ambient temperature for January.

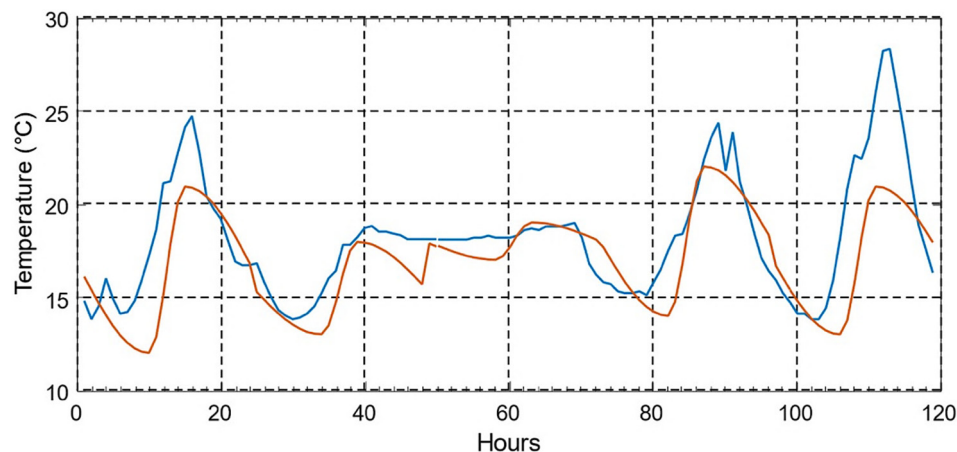
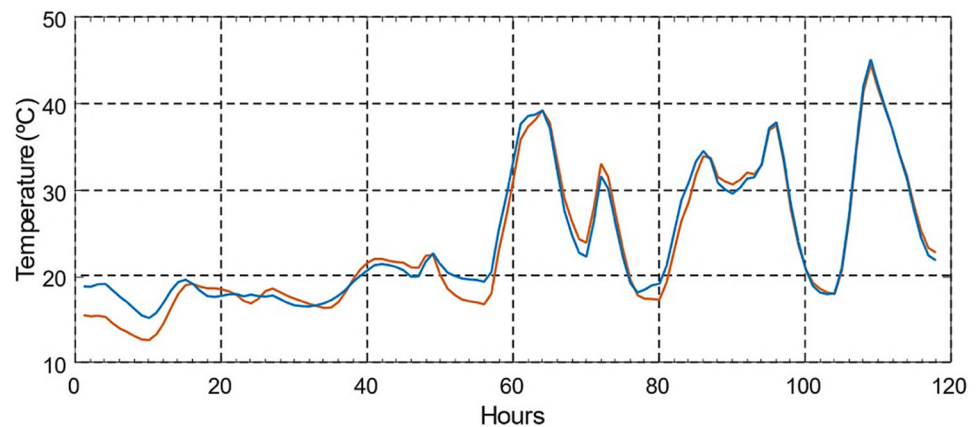


Figure 41. Simulated (blue) and measured (orange) ambient temperature for August.

Table 21. Error between simulated and measured temperature.

	January	August
Error Root Mean Square (ERMS)	1.5 °C	2.3 °C
Absolute Mean Error (AEM)	1.25 °C	1.63 °C
Relative Mean Error (RME)	20.18%	8.53%

By observing Figures 41 and 42 and Table 21, it can be seen that the simulation leads to small errors between the simulated and measured ambient temperature. However, to confirm that the ambient temperature simulation leads to realistic estimates of the top oil temperature and the hotspot temperature, these were estimated using the simulated ambient temperature and the measured ambient temperature. To apply the thermal model, it was still necessary to define the characteristic parameters of the transformer to be used in the model, as it is only known that the type of cooling is ONAF. The parameters to be used in the model correspond to those of this cooling type, as mentioned in Equation (8) in Table 11. Thus, it is possible to estimate the oil temperature at the top of the transformer and in the hotspot with all the data necessary for applying the thermal model.



**Figure 42.** Oil temperature at the top of the oil through simulated (blue) and measured (orange) ambient temperature for January.

Figures 42 and 43 show the evolution of the top oil temperature and the hotspot temperature for the first week of January, while Figures 44 and 45 show the same for August. The blue represents estimates using the measured ambient temperature, and the orange is the simulated one from the thermal model. For these estimations, five-day load factor data from online data were used.

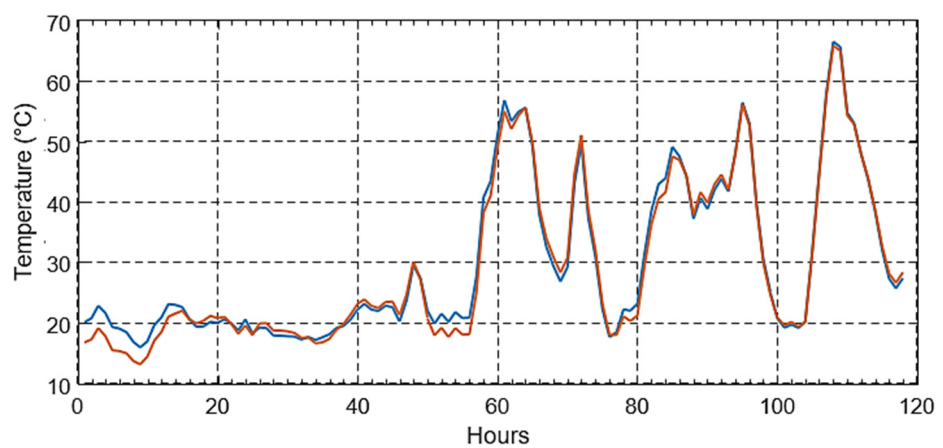


**Figure 43.** Hot-spot temperature through simulated (blue) and measured (orange) ambient temperature for January.

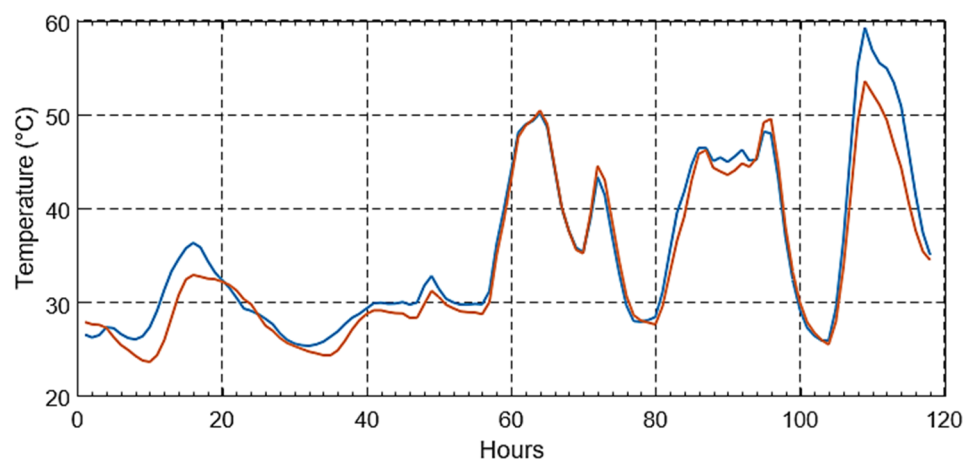


**Figure 44.** Oil temperature at the top of the transformer through simulated (blue) and measured (orange) ambient temperature for August.

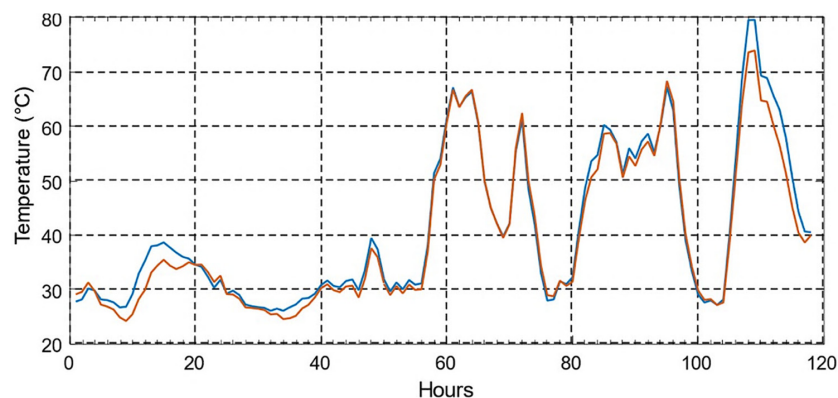


**Figure 45.** Hot-spot temperature through simulated (blue) and measured (orange) ambient temperature for August.

Table 22 lists the errors of the estimates made by the thermal model using the simulated ambient temperature and the ambient temperature measured for January and August. It should be noted that the errors for the hotspot and top-oil temperature are the same. So only one value is shown for each error for January and August.

**Table 22.** Errors between estimated and measured temperature.

	January	August
<b>Error Root Mean Square (ERMS)</b>	1.51 °C	2.17 °C
<b>Absolute Mean Error (AEM)</b>	1.16 °C	1.54 °C
<b>Relative Mean Error (RME)</b>	4.79%	3.74%

It is thus proved, by observing Figures 42–45 and Table 22, that, in the absence of records of ambient temperature, it is possible to simulate the same using daily records from a location at a considerable distance. The results of the model temperature lead to a minimal error when comparing results using measured and simulated ambient temperatures.

Figure 46 shows the temperature available in the online data (blue) and the estimated temperatures of the top oil (orange) and hotspot (yellow). The time base was hourly. For this, hourly averages of the data were calculated every 2 min. It is verified that the temperature available in the online data presents an identical variation to the estimated temperatures, although with a smaller amplitude. The cooling system monitoring would then compare the measured and estimated temperatures. However, as the location of the temperature available in the online data (blue) is not known, the comparison became not valid.

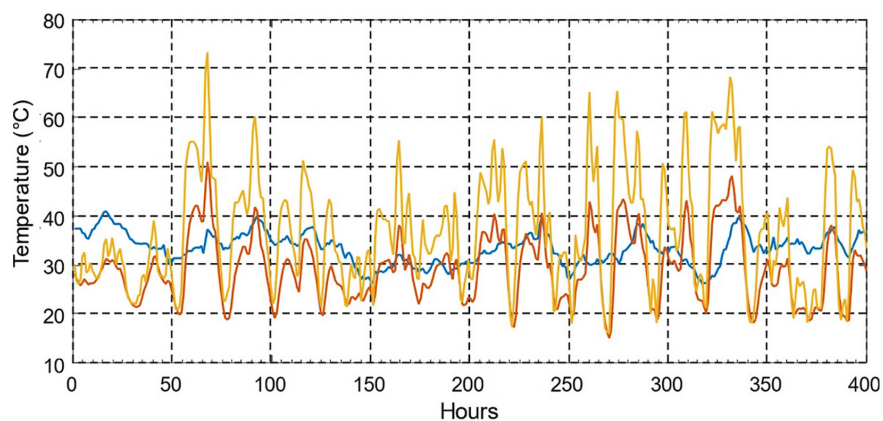


**Figure 46.** Temperature was available in online data (blue) and estimated top oil (orange) and hot spot (yellow) temperatures.

### 5.9. Model for Estimating the Water Content of the Insulation (Paper and Cardboard) and Temperature of the Water Bubbles

The implementation of this model, already described in Section 4.3, is limited because the temperature of the oil in the Hydrocal chamber is not measured when measuring the water content. The temperature available in the online data was then used to approximate Equation (17). The top of the oil's estimated temperature was used for the remaining equations.

One verified an average of 4 to 5 water-in-oil measurements per day. This can vary greatly depending on the temperature. Hence, we calculated a water-on-paper value for each water-in-oil measurement using the available temperature corresponding to the hour of measurement. If the water content in the oil is measured at 14:34, the temperature to be used in the equations is the temperature at 14:00, which corresponds to an average of the temperatures available between 14:00 and 15:00. After having the water content values in the paper for several hours of measuring water in the oil, daily averages were made, thus obtaining a value for each day. Then, weekly averages were performed, that is, averages with values every seven days and averages weighing the seven days before each measurement.

Figure 47 shows the water content in the paper for each day in blue, the average of each measurement day weighing the previous seven days is shown in orange, and the average points taken every seven days are shown in black circles. These points were placed on day four, approximately in the middle of the seven days.

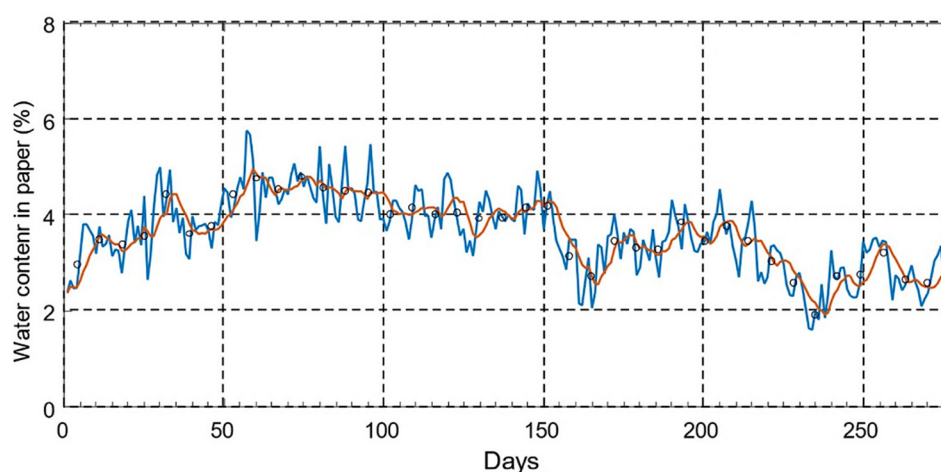


**Figure 47.** Evolution of water content in the paper. Water content in the paper is in blue, the average of each measurement day weighing the previous seven days is shown in orange, and the average points taken every seven days are shown in black circles.

The water content in the paper is a little more variable than supposed, which is justified by the temperature-related limitations mentioned before. Figure 47 shows that the water content exceeds the acceptable limit suggested in the IS 10593 standard for this transformer, which corresponds to 1.25%. However, one cannot be sure of the results because the water content values in the oil *online* and *offline* are quite discrepant. The square root of the mean squared error takes the value 0.3313% for days with average values every seven days and averages weighting the previous seven days for days where there are blue and black dots. As the value of the square root of the root-mean-square error is small compared to the amplitude of values and visually, both averages are very close, it is concluded that it is possible to have a value of water content in the paper for every day, through weighted averages the previous seven days.

With the water content data in the paper, it is then possible to estimate the temperature at which bubble formation risks using Equation (21). For constants  $A$  and  $B$ , values were defined for used Shell Diala K 6 SX oil and thermally improved paper. Although the oil is

different, it is believed that the characteristics are similar and do not significantly impact the result because oils for transformers must comply with certain standards.

Figure 48 shows the evolution of the limit temperature of risk of water bubble formation in blue and the hot-spot temperature estimated through the thermal model in orange. There are no estimated values for the water bubble formation temperature every hour because there are no water content measurements in the oil every hour. However, as the water content variation in the paper is very small, the limit variation will also be. Observing the figure, it can be concluded that there was no formation of bubbles since the transformer temperature never reached values close to the bubble formation temperature limit.

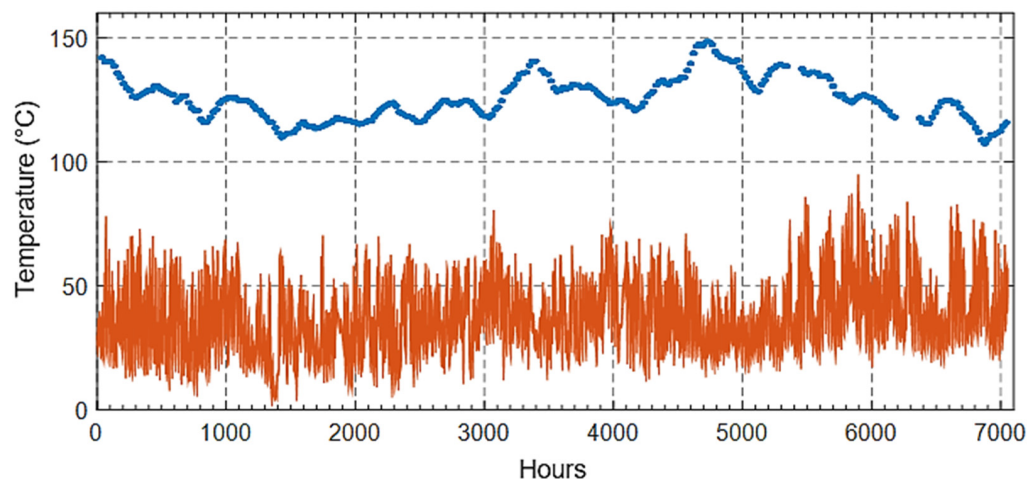


**Figure 48.** The evolution of bubble formation threshold temperature (blue) and the estimated hotspot temperature (orange).

#### 5.10. Transformer Aging Model

For the aging model, it is necessary to have the water content in the paper and the oxygen concentration as input data, as described in Section 4.3. Hydrocal and its estimation do not measure the oxygen concentration through multiple linear regression, as is done for other gases in Section 5.12, which has a large inherent error. The approach followed was to interpolate the oxygen from the *offline* data.

A vector was then created with the days from the date of commissioning of the transformer to that date plus sixty years, which corresponds to the average life expectancy of the transformers. This value was assigned to the online data for the days that offline oxygen measurement was available. For days when the offline measurement is unavailable, the value of the previous measurement was assigned, except for cases in which there was no measurement (the first ones). The value of the first measurement was assigned. The oxygen concentration is *online* and thus has the evolution represented in Figure 49. Only four years are represented because, backward and forwards, the values extend. This approach was chosen because the oxygen levels that define constant *A* cover a large range of values. As the variation in oxygen concentration between measurements is generally relatively small, it is concluded that this interpolation approach leads to a small error in selecting oxygen levels.

With the concentration of oxygen and water in the solid insulation, it is possible to determine the constant *A* for the days when both measurements are made, from November to August. For the period after the absence of water values in solid insulation, constant *A* is taken as the last to be calculated. In contrast, for the period before the existence of values, constant *A* was taken as the value corresponding to 0.5% of water content in the paper and low oxygen concentration. Since the initial value of the degree of polymerization was not available, the value of 1200 was assumed since the expected initial value is 1100/1200. The estimated hot-spot temperature is used in the Arrhenius Equation (2). For the days when this is not estimated, the average of the same was assumed.

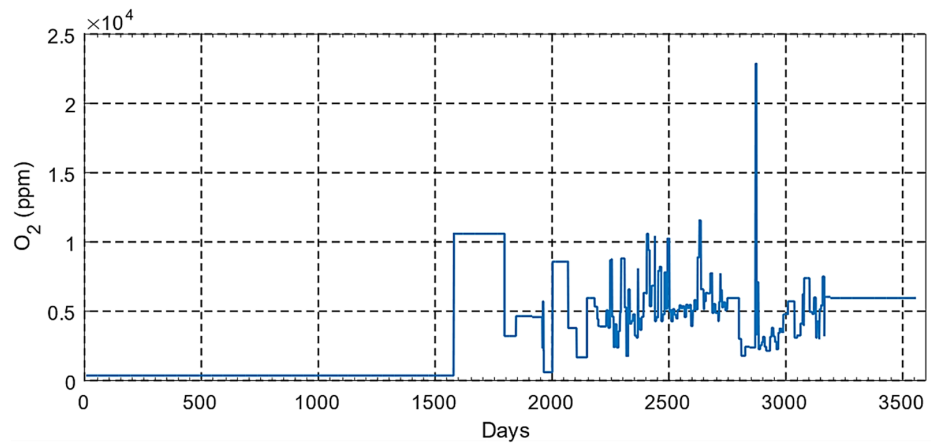


Figure 49. Evolution of interpolated oxygen concentration for online data.

With all input variables defined, the evolution of the degree of polymerization was simulated, which can be seen in Figure 50. This represents the evolution up to sixty years after the commissioning date (blue). It also represents the mortality limit (red). Figure 51 shows a portion of the graph in Figure 50 (orange circle) corresponding to the days when you have water content values in the solid insulation. Here it is possible to observe the daily variation of the aging rate. It is thus verified that it is possible to update the curve of the degree of polymerization daily to have an approximate perception of the state of the solid insulation continuously over time. For this, it is necessary to have the value of water content in the paper, the oxygen concentration, and the hot-spot temperature each day, which can be estimated by the thermal model, as is the case.

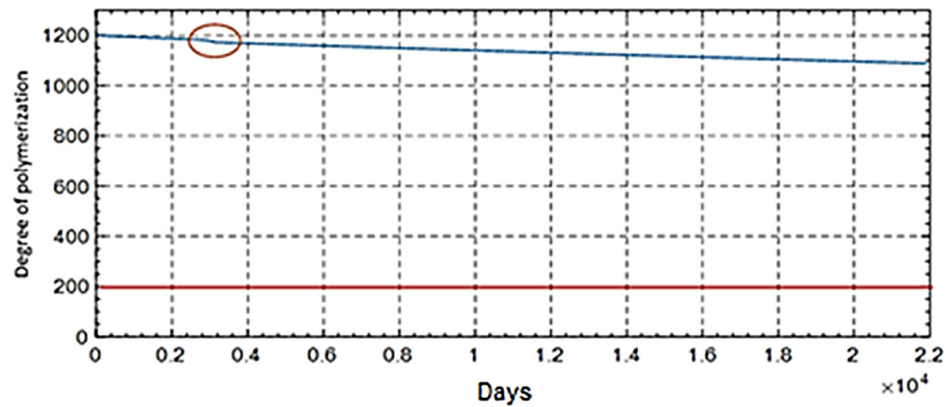


Figure 50. Simulation of the degree of polymerization since the transformer’s commissioning date.

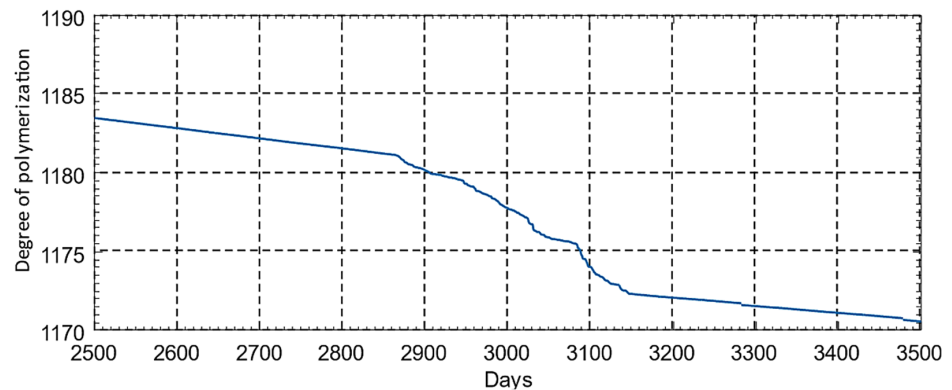
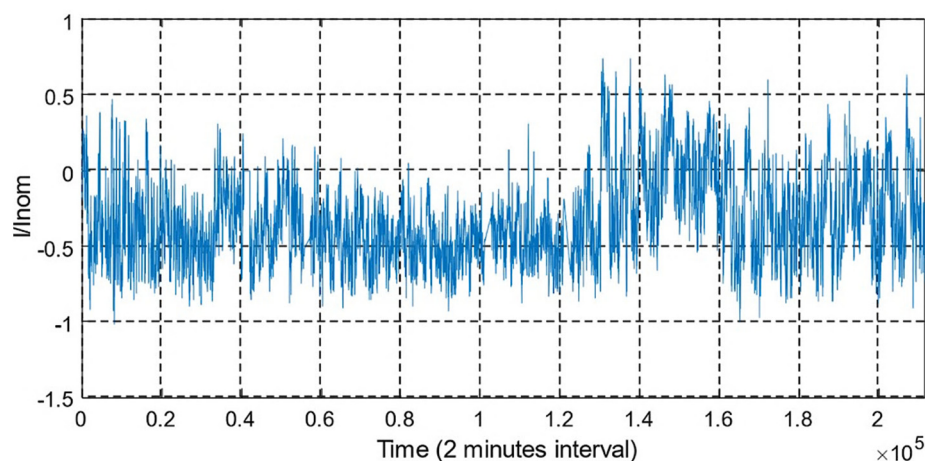


Figure 51. Simulation of the degree of polymerization for days in which there are data on the water content in the paper.

### 5.11. Load Factor Model

The load model aims to verify whether the load exceeds the limit of 200%, in which case the load factor must be between  $-2$  and  $2$ . As shown in Figure 52, the evolution of the load factor can be seen. Charge every 2 min, and the charge never exceeds the specified limit, so no alarm should “sound.”



**Figure 52.** Evolution of the load factor.

### 5.12. Model for Analysis of Gases Dissolved in Oil

To apply the analysis methods of gases dissolved in oil to the online data, the concentration of  $\text{CH}_4$ ,  $\text{C}_2\text{H}_6$  and  $\text{CO}_2$  was estimated. Firstly, it was observed from the offline data that there is a strong correlation between some gases, as shown in Table 23. As in the online data, the gases measured are  $\text{H}_2$ ,  $\text{C}_2\text{H}_2$ ,  $\text{C}_2\text{H}_4$ , and  $\text{CO}$ . It is only important to understand which not measured gases are most correlated. The correlations considered significant between existing and non-existent gases in the online data are highlighted in green in the table. It is concluded that of the gases that do not exist in the online data, only  $\text{N}_2$  and  $\text{O}_2$  do not present significant correlations with the gases in the online data. However, they present a strong correlation between them.

**Table 23.** Correlation between gases measured by specialized laboratory (*offline*). The green color marks a strong correlation between some gases.

	$\text{H}_2$	$\text{O}_2$	$\text{N}_2$	$\text{CO}$	$\text{CO}_2$	$\text{CH}_4$	$\text{C}_2\text{H}_4$	$\text{C}_2\text{H}_6$	$\text{C}_2\text{H}_2$
$\text{H}_2$	1.00	−0.057	0.033	0.347	0.433	0.635	0.576	0.6353	0.717
$\text{O}_2$	−0.057	1.00	0.913	0.1922	0.308	−0.143	−0.150	−0.126	0.0486
$\text{N}_2$	0.033	0.914	1.00	0.288	0.399	−0.15	−0.167	−0.129	0.135
$\text{CO}$	0.347	0.192	0.2885	1.00	0.794	−0.293	−0.348	−0.275	0.387
$\text{CO}_2$	0.433	0.308	0.399	0.794	1.00	0.021	0.002	0.056	0.553
$\text{CH}_4$	0.635	−0.143	−0.151	−0.29	0.021	1.00	0.993	0.994	0.332
$\text{C}_2\text{H}_4$	0.576	−0.15	−0.168	−0.348	0.002	0.993	1.00	0.989	0.319
$\text{C}_2\text{H}_6$	0.635	−0.126	−0.129	−0.275	0.057	0.994	0.989	1.00	0.327
$\text{C}_2\text{H}_2$	0.717	0.048	0.135	0.387	0.553	0.332	0.31	0.327	1.00

To estimate the  $\text{CH}_4$  concentration, one started by using  $\text{C}_2\text{H}_4$  as the input variable since this is the one that has the highest correlation with  $\text{CH}_4$ , having obtained the following expression  $\text{CH}_4 = -5.815 + 0.9\text{C}_2\text{H}_4$ . Then, the  $\text{CH}_4$  concentration was estimated for the various days when  $\text{C}_2\text{H}_4$  values were available in the online data. After this step, the mean squared error square root between the estimated online and offline data was calculated for the measured dates, 43.48 ppm. We proceeded analogously but added  $\text{H}_2$  to the model,

obtaining a square root of the mean square error of 40.24 ppm. By adding  $C_2H_2$  to the model, the square root of the root-mean-square error became 39.46. This last improvement of the model was considered insignificant, having chosen the model in which  $CH_4$  is estimated from  $H_2$  and  $C_2H_4$ .

The model is then described by the expression  $CH_4 = -10.057 + 0.8782C_2H_4 + 0.064H_2$ , which has a coefficient of determination ( $R^2$ ) equal to 0.9963; approximately 99.63% of the cause of the  $CH_4$  concentration is due to the concentration of  $C_2H_4$  and  $H_2$ . The model variables have a high level of significance, thus showing that it is unlikely that there is no relationship between the concentration of  $CH_4$  and the concentration of  $C_2H_4$  and  $H_2$ . The model also has a p-value much smaller than 0.01, leading to the rejection of the null hypothesis, which complements the presented hypothesis.

In the graph of Figure 53, the values estimated by the linear model for the  $CH_4$  concentration through the online  $C_2H_4$  and  $H_2$  values are represented in blue, and the  $CH_4$  concentration values from the offline data are shown in orange. It is concluded that both data values are very close, with a greater difference from approximately day 200 onwards. It is still possible to observe three distinct zones observed for  $C_2H_4$ .

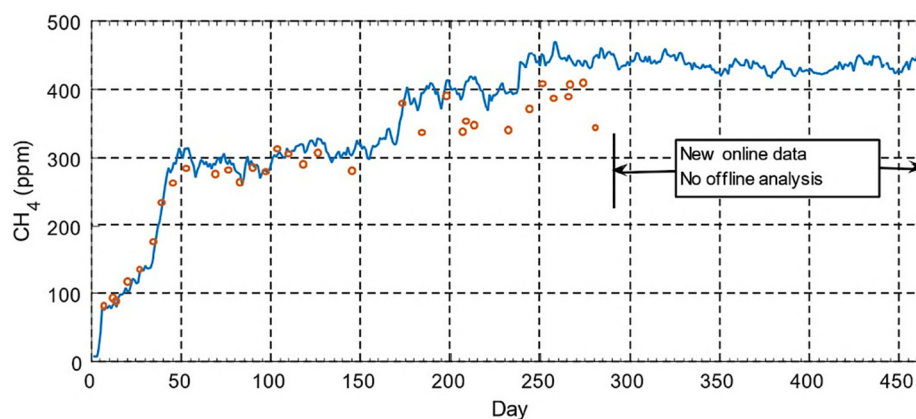


**Figure 53.** Evolution of methane concentration over time, *online* (blue) and *offline* (orange) data.

Similarly, the concentration of  $C_2H_6$  was estimated, concluding that the linear model that leads to the best results for its estimation has  $C_2H_4$  and  $C_2H_2$  as input variables. The model has the following expression  $C_2H_6 = 1.572 + 0.188C_2H_4 + 0.0244C_2H_2$ . The coefficient of determination takes the value of 0.9923, and the p-value is much smaller than 0.01. It is also verified that  $C_2H_4$  has a significance level higher than  $C_2H_2$ . Figure 54 shows the evolution of the estimated  $C_2H_6$  concentration for online (blue) and the offline values (orange) measured by the specialized laboratory. Almost similar behavior is seen between online (estimated) and offline data.

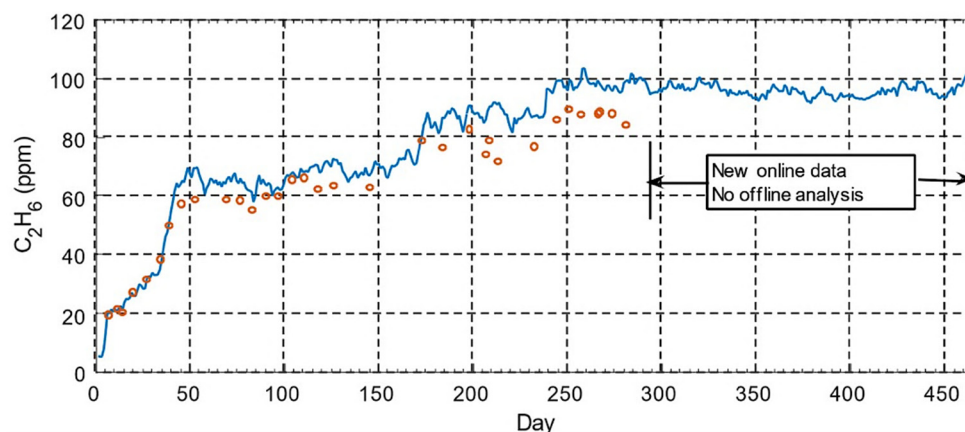


**Figure 54.** Evolution of ethane concentration over time, *online* (blue) and *offline* (orange) data.

Finally, the CO<sub>2</sub> concentration was estimated for online data using the same procedure. The model is given by  $\text{CO}_2 = 133.986 + 0.258\text{H}_2 + 2.688\text{CO}$ , and both variables have high levels of significance, a coefficient of determination of 0.7769, and a p-value much lower than 0.01. Figure 55 shows the evolution of the gas for online (blue) and offline (orange) data, proving an approximate behavior between the two, in which the gas increases almost constantly over time.

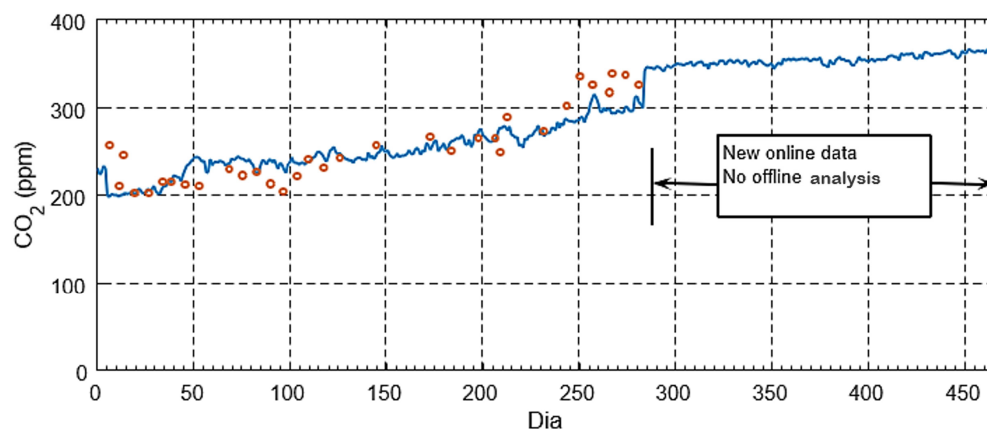


**Figure 55.** Evolution of carbon dioxide concentration over time, *online* (blue) and *offline* (orange) data.

Table 24 shows the errors between the estimated online data and the measured offline data for the dates. The errors are significant, mainly for methane. It should be noted that the errors found for these three estimated gases result from the error between the concentrations of the measured online and offline measured gases.

**Table 24.** Errors between online estimation and offline measurements of gas concentration.

Gases	Error Root Mean Square (ERMS)	Absolute Mean Error (AEM)	Relative Mean Error (RME)
CH <sub>4</sub>	40.24 ppm	30.85 ppm	10.13%
C <sub>2</sub> H <sub>6</sub>	8.3 ppm	6.82 ppm	9.75%
CO <sub>2</sub>	23.13 ppm	17.95 ppm	6.93%

After estimating the concentration of these gases, it is then possible to apply the analysis methods of gases dissolved in the oil to the online data and compare the results with the offline data for the dates on which there is information on both.

Before applying the methods to the online data, it is necessary to define the limits for the concentration of gases and the rate of change. As it is intended to compare the results of applying the methods of analysis of gases dissolved in oil to the online data with the offline data, the limits to be imposed will be the same as those of the specialized laboratory. It was verified that the limits used by the specialized laboratory are those of the IEEE C57.104 standard referenced in Table 14. It was also verified that although some comments verified that the stabilization of the concentrations of the gases is an important factor, the rate of variation is not a condition for applying the methods. The only condition the laboratory checks to apply the methods is the limit of concentrations, which even makes sense since sampling is much longer than thirty days in some situations. Thus, it was decided to apply the methods to the online data, imposing and not the condition of the variation rate. As mentioned in Section 4.5, it must be greater than 10% when comparing the day under analysis with the day thirty days before.

The methods applied by the specialized laboratory, the Duval and IEC methods, were also applied to the online data, with and without applying the rate of change condition. Figures 56 and 57 make it possible to visualize the evolution of failures according to the

Duval and IEC method, respectively, over time. It was decided to put the evolution of failures in a graph due to the large volume of data. It was necessary to encode the failures with numbers. The failure coding is present in Table 25. The days are not temporally consecutive until the 95th day, where there is only offline data, points in yellow. The sampling of offline data is not daily and is very variable. Thus, in these first 95 days, there were faults between 2008 and 2014. From day 95 onwards, the days are temporally followed for both sampling periods, and despite being temporally spaced, it was decided to unite both periods graphically. The first online sampling period is between day 96 and day 378, and the second is between day 97 and day 561. The two blue lines in the figure refer to online data, and the dark blue line does not consider the condition of the rate of change, while the other does. The blue line is the same as the dark blue line except when it transitions to zero, indicating no fault. The rate of change was determined for the first 30 days of online data by comparing the closest offline data from a previous month to the online days under analysis. Between the online data periods, it was assumed that these would be followed, as they were spaced two months, and the concentrations of the gases vary very little in the transition of periods.

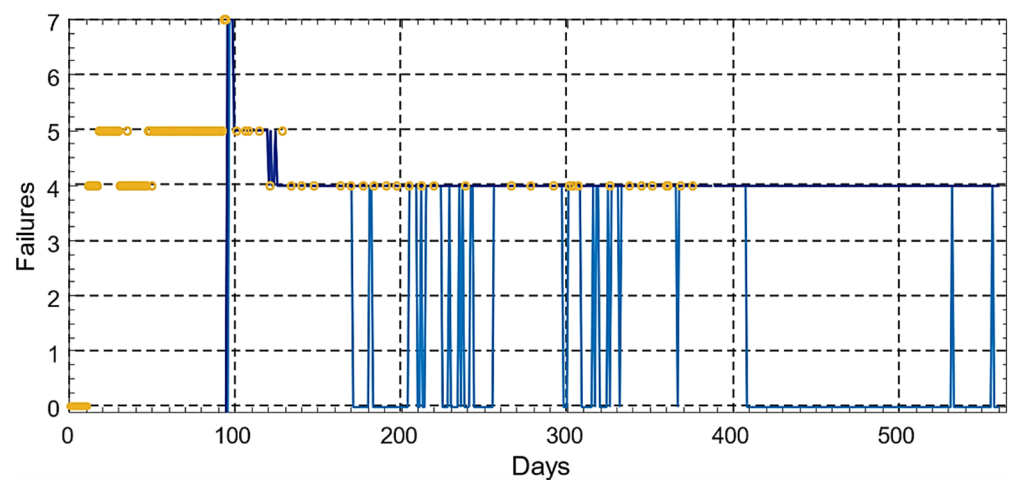


**Figure 56.** Evolution of failures according to Duval's method for *offline* (yellow), *online* without (dark blue), and with (blue) change rate conditions.

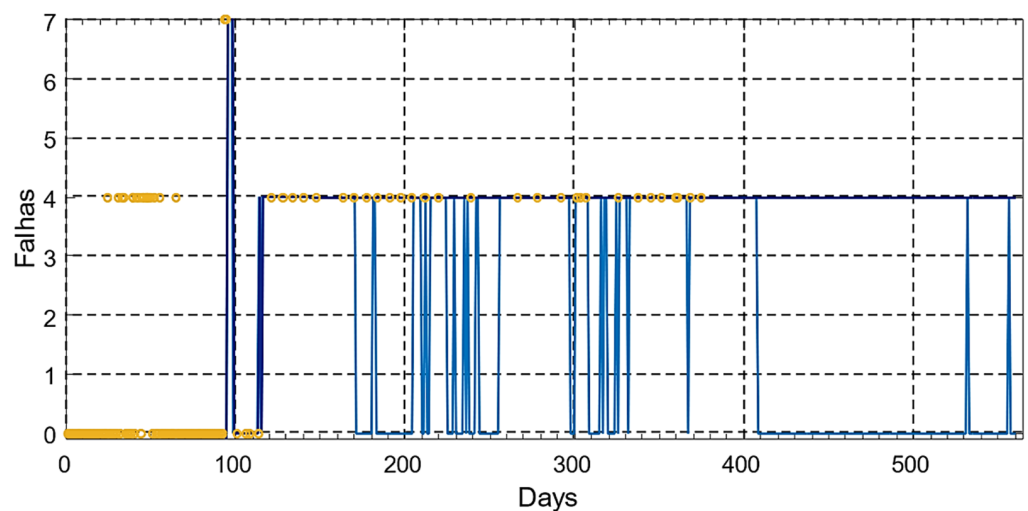


**Figure 57.** Evolution of failures according to the IEC method for *offline* (yellow), *online* without (dark blue), and with (blue) change rate conditions.

**Table 25.** Codification of types of failures.

Code	Failure Type
0	No failure
1	partial discharges
2	Thermal [150–300 °C]
3	Thermal [300–700 °C]
4	Thermal [>700 °C]
5	Electrical evasion and thermal failure
6	low energy discharge
7	High energy discharge (Arc-electric)

Observing the evolution of the failures in Figures 56 and 57, it can be concluded that both online data, in dark blue and offline data, show the same trend, proving the reliability of the online data. Thus, although the concentrations of gases online and offline are sometimes a little discrepant, the final result is the same. For the online data in blue, it can be seen that in some of the times that the others suggest failure, this one does not, which even makes sense because observing the evolution of the gases in Section 5.6 and this one, it can be seen that they stabilize in some periods, as well as in these periods it appears that the fault has disappeared. It is then concluded that the approach of inserting the rate of change condition leads to more realistic results. However, it is impossible to determine the cause of these failures as there is no data to evaluate all the components. In addition, as is the case with the estimation model of water content in the insulation (paper and cardboard), it is not certain whether all results were obtained due to the mentioned limitations.

## 6. Conclusions

In this paper, a review and analysis of the continuous methods of monitoring and diagnosis of large-power transformers were carried out, where some techniques that enable their implementation were demonstrated. The main components of a large-power transformer and the abnormal operating conditions that usually arise were revised. Traditional methodologies for diagnosing power transformers, in general, were also reviewed, having verified the existence of different techniques to determine the condition of each of the main components of the transformer. After, a set of models (thermal, water content in the oil, aging, etc.) for continuously monitoring and diagnosing the power transformer was presented.

All previous techniques and models were applied to an existing large-power transformer consisting of a phase-shifting 1400 MVA 400 kV three-phase transformer. It has been available to study with record data of its service since 2007. The continuous data made available from the phase-shift transformer were presented, and the monitoring and diagnosis models were applied to them.

It was verified in some gas concentration values measured at the transformer the existence of discrepancies between the data obtained by the DGA device and the data obtained by a specialized laboratory. Some gases crucial to applying analysis methods of gases dissolved in oil were not measured. Thus, using linear regressions obtained through the gases quantified by the specialized laboratory, it was possible to estimate the missing gases concentration and use them in the models, which presented very close results to the results obtained by the laboratory.

Based on the previous models and records of maximum and minimum ambient temperature measured near the transformer, it was possible to determine the hotspot temperature and the oil temperature on the top of the transformer.

We can conclude that online diagnostic models are critical to monitoring and diagnosing power transformers, thus becoming an asset for entities that manage energy networks

today. They allow continuous access over time and automatically to the condition of their set of large power transformers. Thus, they can act when an anomaly occurs in the transformer, avoiding technical and economic costs that can be quite high and even better managing the transformer's life cycle.

It will be interesting to report the transformer's internal and external variables with more data. It was found, for example, that there is a strong relationship between transformer temperature, ambient temperature, and wind speed. Through weather forecasts, it could be possible to predict the temperature of the transformer. It will also be important to develop a model for monitoring the windings using the ratio of the number of turns as a load function and the transformer's history, namely failures and continuous data over time. Doing this will be possible to associate them and remove patterns to predict the occurrence of failures.

**Author Contributions:** Conceptualization, P.J.C.B. and D.F.F.d.S.; methodology, P.J.C.B.; software, D.F.F.d.S.; validation, D.F.F.d.S.; formal analysis, P.J.C.B.; investigation, P.J.C.B., D.F.F.d.S. and J.V.C.; data curation, D.F.F.d.S.; writing—original draft preparation, D.F.F.d.S.; writing—review and editing, J.V.C.; visualization, J.V.C.; supervision, P.J.C.B.; project administration, P.J.C.B. All authors have read and agreed to the published version of the manuscript.

**Funding:** This work was partially financed by national funds through FCT—Foundation for Science and Technology, I.P., through IDMEC, under LAETA, project UIDB/50022/2020.

**Institutional Review Board Statement:** Not applicable.

**Informed Consent Statement:** Not applicable.

**Data Availability Statement:** Not applicable.

**Conflicts of Interest:** The authors declare no conflict of interest.

## References

1. CIGRE Technical Brochure 248. *Economics of Transformer Management*; June 2004. Available online: <https://e-cigre.org/publication/248-economics-of-transformer-management> (accessed on 12 May 2022).
2. Office of Electricity Delivery & Energy Reliability. *Large Power Transformers and the U.S. Electric Grid*; Office of Electricity Delivery & Energy Reliability: Washington, DC, USA, 2012.
3. USITC. *Large Power Transformers from Korea*; USITC: Washington, DC, USA, 2011.
4. Westman, T.; Lorin, P.A.; Ammann, P.A. Keeping aging transformers healthy for longer with ABB TrafoAsset Management—Proactive Services. *ABB Rev.* **2010**, *1*, 63–69.
5. Bossi, A.; Dind, J.E.; Frisson, J.M.; Khoudiakov, U.; Light, F.H.; Narke, D.V.; Tournier, Y.; Verdon, J. An international survey on failures in large power transformers. *Cigré Electra* **1983**, *88*, 21–48.
6. Special Report: Large Power Transformers and the U.S. Electric Grid, the Infrastructure Security and Energy Restoration Office of Electricity Delivery and Energy Reliability, U.S. Department of Energy, June 2012. Available online: [https://www.energy.gov/sites/prod/files/Large%20Power%20Transformer%20Study%20-%20June%202012\\_0.pdf](https://www.energy.gov/sites/prod/files/Large%20Power%20Transformer%20Study%20-%20June%202012_0.pdf) (accessed on 7 March 2022).
7. Bohatyrewicz, P.; Mrozik, A. The Analysis of Power Transformer Population Working in Different Operating Conditions with the Use of Health Index. *Energies* **2021**, *14*, 5213. [[CrossRef](#)]
8. Aslam, M.; Haq, I.U.; Rehan, M.S.; Ali, F.; Basit, A.; Khan, M.I.; Arbab, M.N. Health Analysis of Transformer Winding Insulation Through Thermal Monitoring and Fast Fourier Transform (FFT) Power Spectrum. *IEEE Access* **2021**, *9*, 114207–114217. [[CrossRef](#)]
9. Bagheri, M.; Naderi, M.S.; Blackburn, T.; Phung, T. FRA vs. short circuit impedance measurement in detection of mechanical defects within large power Transformer. In Proceedings of the Conference Record of the IEEE International Symposium on Electrical Insulation (ISEI), San Juan, PR, USA, 10–13 June 2012; pp. 301–305.
10. Wang, S.; Wang, S.; Cui, Y.; Long, J.; Ren, F.; Ji, S.; Wang, S. An Experimental Study of the Sweep Frequency Impedance Method on the Winding Deformation of an Onsite Power Transformer. *Energies* **2020**, *13*, 3511. [[CrossRef](#)]
11. Cong, H.; Pan, H.; Hu, X.; Zhang, M.; Li, Q. Micro-mechanism study on synergistic degradation of the oil-paper insulation with dibenzyl disulfide, hexadecyl mercaptan and benzothiophene. *High Volt.* **2020**, *6*, 448–459. [[CrossRef](#)]
12. Sweetser, C. Power Transformer Diagnostics: Novel Techniques and their Application. In Proceedings of the OMICRON, Technical Meeting, 2016. Available online: <https://pt.scribd.com/document/400147838/Charles-Sweetser-XFMR-Testing> (accessed on 12 May 2022).
13. Teymouri; Ashkan; Vahidi, B. Power transformer cellulosic insulation destruction assessment using a calculated index composed of CO, CO<sub>2</sub>, 2-Furfural, and Acetylene. *Cellulose* **2021**, *28*, 489–502. [[CrossRef](#)]

14. Brandtzæg, G. Health Indexing of Norwegian Power Transformers. Thesis in Engineering of Energy and Environment. Master's Thesis, Norwegian University of Science and Technology, Trondheim, Norway, 2015.
15. Ansari, M.A.; Martin, D.; Saha, T.K. Advanced Online Moisture Measurements in Transformer Insulation Using Optical Sensors. *IEEE Trans. Dielectr. Electr. Insul.* **2020**, *27*, 1803–1810. [[CrossRef](#)]
16. Adusumilli, P.; Sundar, S.V.N.J. A new criterion for optimal dielectric design of high voltage bushing internal shields in large power transformer. In Proceedings of the 2019 International Conference on High Voltage Engineering and Technology (ICHVET), Hyderabad, India, 7–8 February 2019.
17. Xie, Q.; He, C.; Yang, Z.; Wen, J. Tests and analyses on failure mechanism of 1100 kV UHV transformer porcelain bushing. *High Volt. Eng.* **2017**, *43*, 3154–3162.
18. Walczak, K.; Gielniak, J. Temperature Distribution in the Insulation System of Condenser-Type HV Bushing—Its Effect on Dielectric Response in the Frequency Domain. *Energies* **2021**, *14*, 4016. [[CrossRef](#)]
19. Wang, D.; Zhou, L.; Yang, Z.; Liao, W.; Wang, L.; Guo, L. Simulation for transient moisture distribution and effects on the electric field in stable condition: 110 kV oil-immersed insulation paper bushing. *IEEE Access* **2019**, *7*, 162991–163002. [[CrossRef](#)]
20. Li, S.; Yang, L.; Li, S.; Zhu, Y.; Cui, H.; Yan, W.; Ge, Z.; Abu-Siada, A. Effect of AC-voltage harmonics on oil impregnated paper in transformer bushings. *IEEE Trans. Dielectr. Electr. Insul.* **2020**, *27*, 26–32. [[CrossRef](#)]
21. Liu, J.; Yang, S.; Zhang, Y.; Zheng, H.; Shi, Z.; Zhang, C. A modified X-model of the oil-impregnated bushing including non-uniform thermal aging of cellulose insulation. *Cellulose* **2020**, *27*, 4525–4538. [[CrossRef](#)]
22. Redmil, Presentation on the Slideshare Website. Available online: <http://pt.slideshare.net/rezzmk/redmil-powerpoint> (accessed on 20 December 2015).
23. Ndiaye, I.; Betancourt Ramírez, E.; Avila Montes, J.; Jiang, Y.; Elasser, A. *Grid Ready, Flexible Large Power Transformer*; No. Final Technical Report: DE-OE0000852; GE Global Research: Niskayuna, NY, USA, 2019.
24. Dohnal, D. *On-Load Tap-Changers for Power Transformers*; Maschinenfabrik Reinhausen GmbH Falkensteinstrasse: Regensburg, Germany, 2013; Volume 8, p. 93059.
25. Handley, B.; Redfern, M.; White, S. On load tap-changer conditioned based maintenance. *IEE Proc.-Gener. Transm. Distrib.* **2001**, *148*, 296–300. [[CrossRef](#)]
26. Al-Ameri, S.M.; Alawady, A.A.; Yousof MF, M.; Kamarudin, M.S.; Illias, H.A. The Effect of Tap Changer Coking and Pitting on Frequency Response Analysis Measurement of Transformer. In Proceedings of the 2021 IEEE International Conference on the Properties and Applications of Dielectric Materials (ICPADM), Johor Bahru, Malaysia, 12–14 July 2021.
27. Seo, J. Intelligent condition monitoring and diagnosis of a power transformer: On-load tap changer (OLTC) and main winding. Ph.D. Thesis, The University of Queensland, St Lucia, Australia, 2019.
28. Saha, T.K.; Purkait, P. (Eds.) *Transformer Ageing: Monitoring and Estimation Techniques*; John Wiley & Sons: Hoboken, NJ, USA, 2017.
29. Brodeur, S.; Lê Van, N.; Champliand, H. A nonlinear finite-element analysis tool to prevent rupture of power transformer tank. *Sustainability* **2021**, *13*, 1048. [[CrossRef](#)]
30. Jahromi, A.; Piercy, R.; Cress, S.; Service, J.; Fan, W. An approach to power transformer asset management using health index. *IEEE Electr. Insul. Mag.* **2009**, *25*, 20–34. [[CrossRef](#)]
31. Wang, R.; Zhang, Y.; Jiao, B. Theory research on high performance control technology of large power transformer strong oil-cooled system. In Proceedings of the 2020 IEEE 4th Information Technology, Networking, Electronic and Automation Control Conference (ITNEC), Chongqing, China, 12–14 June 2020; Volume 1.
32. Kim, Y.J.; Jeong, M.; Park, Y.G.; Ha, M.Y. A numerical study of the effect of a hybrid cooling system on the cooling performance of a large power transformer. *Appl. Therm. Eng.* **2018**, *136*, 275–286. [[CrossRef](#)]
33. Gao, X.; Schlosser, C.A.; Morgan, E.R. Potential impacts of climate warming and increased summer heat stress on the electric grid: A case study for a large power transformer (LPT) in the Northeast United States. *Clim. Chang.* **2018**, *147*, 107–118. [[CrossRef](#)]
34. Weiping, M.; Fangxiao, C.; Ying, S.; Chungui, X.; Ming, A. Fault diagnosis on power transformers using non-electric method. In Proceedings of the 2006 IEEE International Symposium on Industrial Electronics, Montreal, QC, Canada, 9–13 July 2006; Volume 3.
35. Franzén, A.; Karlsson, S. *Failure Modes and Effects Analysis of Transformers*; Royal Institute of Technology, KTH School of Electrical Engineering: Stockholm, Sweden, 2007.
36. Eyüboğlu, O.H.; Dindar, B.; Gül, Ö. Risk Assessment by Using Failure Modes and Effects Analysis (FMEA) Based on Power Transformer Aging for Maintenance and Replacement Decision. In Proceedings of the 2020 2nd Global Power, Energy and Communication Conference (GPECOM), Izmir, Turkey, 20–23 October 2020.
37. Ciulavu, C.; Helerea, E. Power transformer incipient faults monitoring. *Ann. Univ. Craiova-Electr. Eng. Ser.* **2008**, *32*, 72–77.
38. Bustamante, S.; Manana, M.; Arroyo, A.; Laso, A.; Martinez, R. Determination of Transformer Oil Contamination from the OLTC Gases in the Power Transformers of a Distribution System Operator. *Appl. Sci.* **2020**, *10*, 8897. [[CrossRef](#)]
39. Hussain, M.R.; Refaat, S.S.; Abu-Rub, H. Overview and Partial Discharge Analysis of Power Transformers: A Literature Review. *IEEE Access* **2021**, *9*, 64587–64605. [[CrossRef](#)]
40. IEC 60599:2015; Mineral Oil-impregnated Electrical Equipment in Services—Guide to the Interpretation of Dissolved and Free Gases Analysis. International Standard TC 10. IEC: Geneva, Switzerland, 2015.

41. Qi, B.; Zhang, P.; Rong, Z.; Li, C. Differentiated warning rule of power transformer health status based on big data mining. *Int. J. Electr. Power Energy Syst.* **2020**, *121*, 106150. [CrossRef]
42. IEEE Standard C57.104-2008; IEEE Guide for the Interpretation of Gases Generated in Oil-Immersed Transformers. IEEE: Piscataway, NJ, USA, 2008.
43. Cheng, L.; Yu, T. Dissolved Gas Analysis Principle-Based Intelligent Approaches to Fault Diagnosis and Decision Making for Large Oil-Immersed Power Transformers: A Survey. *Energies* **2018**, *11*, 913. [CrossRef]
44. Cheng, L.; Yu, T.; Wang, G.; Yang, B.; Zhou, L. Hot Spot Temperature and Grey Target Theory-Based Dynamic Modelling for Reliability Assessment of Transformer Oil-Paper Insulation Systems: A Practical Case Study. *Energies* **2018**, *11*, 249. [CrossRef]
45. de Faria, H., Jr.; SpirCosta, J.G.; Olivas, J.L.M. A review of monitoring methods for predictive maintenance of electric power transformers based on dissolved gas analysis. *Renew. Sustain. Energy Rev.* **2015**, *46*, 201–209. [CrossRef]
46. Hydroelectric Research and Technical Services Group. *Transformer Diagnostics*; United States Department of the Interior Bureau of Reclamation: Washington, DC, USA, 2003.
47. *DGA Diagnostic Methods, Serveron White Paper, PN 880-0129-00 Rev. B*, Serveron Corporation: Hillsboro, OH, USA, 2007.
48. Atanasova-Höhlein, I. DGA-Method in the Past and for the Future; 2012. Available online: <https://assets.new.siemens.com/siemens/assets/api/uuid:d9fa9803-8a7b-46c0-a9e9-ba0c7af71c29/dga-method-in-the-past-and-for-the-future.pdf> (accessed on 23 June 2022).
49. Dukarm, J.; Draper, Z.; Piotrowski, T. Diagnostic Simplexes for Dissolved-Gas Analysis. *Energies* **2020**, *13*, 6459. [CrossRef]
50. Tahir, M. Intelligent Condition Assessment of Power Transformer Based on Data Mining Techniques Master Thesis. Master's Thesis, University of Waterloo, Waterloo, ON, Canada, 2012.
51. Pickster, K. Determination of Probability of Failure of Power Transformers using Statistical Analysis. Master's Thesis, University of the Witwatersrand, Johannesburg, South Africa, 2015.
52. IEEE Standard C57.106-2006; IEEE Guide for Acceptance and Maintenance of Insulating Oil in Equipment. IEEE: Piscataway, NJ, USA, 2006.
53. Sumeder, C.; Muhr, M. Moisture Determination and Degradation of Solid Insulation System of Power Transformers. In Proceedings of the 2010 IEEE International Symposium on Electrical Insulation, San Diego, CA, USA, 6–9 June 2010; pp. 1–4. [CrossRef]
54. Prevost, T. New Techniques for the Monitoring of Transformer Condition. In Proceedings of the IEEE T&D Conference, Chicago, IL, USA, 17 April 2014.
55. Mohamed, E.A.; Abdelaziz, A.Y.; Mostafa, A.S. A neural network-based scheme for fault diagnosis of power transformers. *Electr. Power Syst. Res.* **2005**, *75*, 29–39.
56. Barle, N.; Jha, M.K.; Qureshi, M.F. Artificial Intelligence Based Fault Diagnosis of Power Transformer-A Probabilistic Neural Network and Interval Type-2 Support Vector Machine Approach. *International Journal of Innovative Research in Science. Eng. Technol.* **2015**, *4*, 71–89.
57. Ahmed, M.R.; Geliel, M.A.; Khalil, A. Power Transformer Fault Diagnosis using Fuzzy Logic Technique Based on Dissolved Gas Analysis. In Proceedings of the 21st Mediterranean Conf. Control Automat. Platania, Greece, 25–28 June 2013; pp. 584–589.
58. Oliveira, L.M.R. *Desenvolvimento de Métodos de Detecção de Avarias e Algoritmos de Proteção para Aplicação em Sistemas de Monitorização Contínua de Transformadores Trifásicos, Tese de Doutoramento*; Faculdade de Ciências e Tecnologia da Universidade de Coimbra: Coimbra, Portugal, 2013.
59. Myers, C. Transformer Conditioning Monitoring by Oil Analysis Large or Small; Contaminant or Catastrophe, in proc. In Proceedings of the First IEE/IMEchE International Conference on Power Station Maintenance-Profitability Through Reliability, Edinburgh, UK, 30 March–1 April 1998.
60. "Engineering Photos, Videos and Articles (Engineering Search Engine)", Chapter 1 Power Transformers. Posted on December 2012. Available online: <http://emadrlc.blogspot.pt/2012/12/chapter-1-power-transformers.html> (accessed on 10 August 2016).
61. Jan, S.T.; Afzal, R.; Khan, A.Z. Transformer Failures, Causes & Impact. In Proceedings of the International Conference Data Mining, Civil and Mechanical Engineering, Bali, Indonesia, 1–2 February 2015.
62. Singh, R.; Zadgaonkar, A.S.; Singh, A. Premature Failure of Distribution Transformers-A Case Study. *Int. J. Sci. Eng. Res.* **2014**, *5*, 1457–1466.
63. University of Coimbra, Physics Department. Available online: [http://www.fis.uc.pt/data/20072008/apontamentos/apnt\\_330\\_15.pdf](http://www.fis.uc.pt/data/20072008/apontamentos/apnt_330_15.pdf) (accessed on 20 December 2015).
64. *Technical Brochure No. 227 Guidelines for Life Management Techniques for Power Transformers. CIGRE WG 12.18; Life Management of Transformers*: Paris, France, 2022; p. 125.
65. Soares, M.A. *Elementos Para a Gestão do Ciclo de Vida de Transformadores Elétricos de Potência, Tese de Mestrado*; FEUP: Porto, Portugal, 2011.
66. ABB, Site da ABB. 2016. Available online: <http://new.abb.com/products/transformers/transformer-components/ac-bushings-iec/oil-to-air-application/ac-bushings-type-gob> (accessed on 20 July 2016).
67. Feilat, E.A.; Metwally, I.A.; Al-Matri, S.; Al-Abri, A.S. Analysis of the Root Causes of Transformer Bushing Failures. *Int. J. Comput. Electr. Autom. Control Inf. Eng.* **2013**, *7*, 791–796.
68. MR, Site da MR. Available online: [http://www.reinhausen.com/desktopdefault.aspx/tabid-1551/179\\_read-335/](http://www.reinhausen.com/desktopdefault.aspx/tabid-1551/179_read-335/) (accessed on 15 June 2016).

- 
69. Franzén, A.; Karlsson, S. *Failure Modes and Effects Analysis of Transformers Technical Report TRITA-EE 2007:040*; KTH School of Electrical Engineering: Zurich, Switzerland, 2007.
  70. Weather Underground Site. Available online: <https://www.wunderground.com> (accessed on 2 March 2022).